Computers and Structures 194 (2018) 97–115

Contents lists available at ScienceDirect

Computers and Structures

journal homepage: www.elsevier.com/locate/compstruc

A data-driven approach to nonlinear elasticity

Lu Trong Khiem Nguyen *, Marc-André Keip

University of Stuttgart, Institute of Applied Mechanics (CE), Chair of Material Theory, Pfaffenwaldring 7, 70569 Stuttgart, Germany

ARTICLE INFO

Article history:
Received 25 January 2017
Accepted 31 July 2017
Available online 27 September 2017

Dedicated to Professor Christian Miehe

Keywords:
Data-driven computational mechanics
Optimization method
Data science
Geometrical nonlinearity
Model-free

ABSTRACT

The so-called distance-minimizing data-driven computing method is extended to deal with boundary-value problems of continuum mechanics within the finite strain theory. In the merit of a data-driven model the solution process is carried out by using directly the experimental data instead of the conventional constitutive laws. Thus it bypasses the uncertainties in fabricating the stress-strain functional relationships from material data. Consequently, the mathematical formulation involves an optimization problem with equality constraints consisting of the equilibrium equations in continuum mechanics and the compatibility conditions on the displacement field. In the framework of finite element formulation the element tangent stiffness, the generalized internal force and the generalized external force can be computed, which renders it amenable to the implementation of finite element procedures. The proposed scheme is validated through the applications to continuum elements and convergence studies of the data-driven solution in regard to the interpolation order, the mesh size as well as the data size. The variational structure allows to recognize the overall pattern of the system of equations to be solved. This includes the structural tangent stiffness and the generalized force vectors.

1. Introduction and background

Data science is emerging with the increasing impact of information technology and the data deluge (Tansley and Tolle [1], Bell et al. [2]). It is being shared among scientists a consensus that data-driven science is considered as the "fourth paradigm" of science after the empirical, theoretical and computational. Although data science can be thought of as emerging from the statistics, which is a large area of mathematics itself, it is now widely accepted that it is rather multi-disciplinary. The techniques and theories behind it are invented from a broad area of mathematics, statistics, operations research, information science and of course computer science (Foreman [3]). To name a few, the term includes optimization problems, database, data mining, machine learning, probability models, pattern recognition and learning, high performance computing and even artificial intelligence. Despite of its tremendous influence on economics, business, finance and recently biological sciences, medical informatics, social sciences, it has had modest impact on materials science and computational mechanics. Perhaps it is because a tremendous effort of looking inside the material structures have brought various models, insights and benefits to computational mechanics. Nevertheless, when it comes to the point when any proposed constitutive laws hardly capture all the aspects of material behaviors, the possibility to embed data directly into the computational models is desirable. For example, the biological tissues exhibit sophisticated mechanical or coupled eletromechanical response to the externally applied conditions. In such scenario the conventionally phenomenological constitutive laws can often be hardly formulated to describe all material aspects. Also, numerical-based experimental data can be produced as long as the micro- or nano-structures of materials are known or assumed. So the material data, which is either accumulated over time through manufactured experiments or numerically produced, tends to grow abundantly with time and with the complexity of the material under consideration.

Basically, the modeling of material behavior is characterized by either curve-fitting data or using hypothesis on the kinematics of the material structures in the framework of multi-scale computations. These parametrization methods aim to reduce the abundance of experimental data to a usable functional relationship between the gradients of primary variables such as deformation gradient, temperature gradient, electric field vector

* Corresponding author.
E-mail addresses: nguyen@mechbau.uni-stuttgart.de (L.T.K. Nguyen), marc-andre.keip@mechbau.uni-stuttgart.de (M.-A. Keip).

http://dx.doi.org/10.1016/j.compstruc.2017.07.031
0045-7949/

and their dual variables such as stress, heat flux and electric displacement vector. In such approach the ultimate target is to reduce a finite but extremely large collection of bits of information to a much smaller number that can still be practically employed.

It is interesting though that a simple example according to Kojic and Bathe showed that residual stresses may be measured at the end of an elastic closed strain path by using the updated Lagrangian Jaumann formulation in the context of hypoelasticity [4].[1] However, when nonlinear elastic models are based on the existence of a stored energy function, the absence of dissipation can be granted (Valanis and Landel [5], Kojic and Bathe [6]). The relation between the dual variables in terms of material data used in this manuscript does not grant the existence of a stored energy, hence the absence of dissipation in general. Undoubtedly, if the data is completely generated in silico through a stored energy function and crowded, we should expect no dissipation after a loading cycle..

The hyperelastic models of Ogden are developed on the basis of strain energy functions using a nonlinear least squares optimization method (Ogden [7]). The proposed form of the strain energy function is usually written in terms of the stretches that can be readily collected from experiments (Ogden et al. [8]). In this manner, one already imposes the specific functional forms of the strain energy function and then utilizes an appropriate least squares optimization to fit the data. Therefore, these approaches involve a global fitting approximation and identification of material parameters in the model. On the one hand the advantage of these models is their easy implementation as long as the material data is available, but on the other, their global features prevent the wide range of application when the data is noisy and drastically oscillated. In order to overcome such disadvantage, Sussman and Bathe proposed to use piecewise spline interpolations of tension-compression test data. They based their computation argument on a strain energy description separable in terms of logarithmic strains and the truncation of series expansion of strain energy in terms of stress values according to Kearsley and Zapas (see [9,10]). This expansion is sometimes referred to as inversion formula. Another mathematically implicit message behind the inversion formula is that for a hyperelasticity model to be uniquely defined both extension and compression parts of a uniaxial test must be taken into account. This statement is highlighted again and physically explained in the work by Latorre et al. [11]. Aside, the What-You-Prescribed-Is-What-You-Get (WYPIWYG) hyperelasticity model is an approach in computing stored energies following the ideas by Sussman and Bathe of employing local interpolations for both the energy and stress-strain data. The Sussman-Bathe model is the first proposed WYPIWYG model, valid for incompressible, isotropic materials. The entire idea of the material model based on spline interpolations or WYPIWYG hyperelasticity is to fit the test data locally with the help of some appropriate inversion formula. It is worthwhile to mention that the WYPIWYG hyperelasticity have been extended to scope the incompressible transversely isotropic materials (Latorre and Mont [12]), orthotropic materials (Latorre and Mont [13]), anisotropic superficial fascia (Lattore et al. [14]) and isotropic compressible materials (Crespo et al. [15]).

Although the lately attempts to describe material behavior are robust and efficient, they share one common feature. The material description is subject to some imposed functional relationship between the kinematic and constitutive variables by using either global or local fitting approximation because spline interpolations are governed by the controlling parameters. With exponentially increasing potential of computers nowadays, it seems that we do not have to sacrifice a large bit of information and that we can benefit from the abundance of material data by incorporating all or a large portion into the mathematical model.

Among the first attempts to overcome the conventional approach, Kirchdoerfer and Ortiz proposed an effective technique to incorporate directly the data into boundary-value problems in the context of continuum mechanics [16]. Their proposed scheme is based on a heuristic variational statement. According to Kirchdoerfer and Ortiz, the merit of the data-driven solver can be briefly recapitulated as follows. The solver aims to find the point in the material data set that minimizes the error violated in satisfying the essential boundary conditions and the conservation laws. Alternatively stated, it finds the point in the constraint set that minimizes a particular distance to the material data set. For this reason we refer to this method as the *distance-minimizing* scheme. The constraint set is comprised of the essential boundary conditions and the conservation laws. A visualization explanation is based on the construction of Voronoi tessellation in the phase space with the material data points as the basis site (Section 2.1 in [16]). Provided that (i) the material data set is countably finite, (ii) the phase is equipped with a well-defined metric, and (iii) the boundary-value problem is well-posed itself, the associated data-driven problem should be well-posed. The optimization problem is performed on a finite set of points. Note that this finite set is not necessarily a vector space.

The visionary work of Kirchdoerfer and Ortiz addresses the linear elasticity problems. That is, the linearized strain tensor and the engineering stress tensor are used in the data-driven model. The scheme has successfully dealt with materially nonlinear mechanical problems. Yet it has not scoped problems where large deformations may occur. Closely relevant, Ibañez et al. have recently introduced a machine learning approach to deal with linear elasticity and inelasticity problems [17]. In their work the locally linear embedding method is applied to the set of material data so that it can be conveniently dealt with in a manifold of lower dimension. Since the material data is available in quite low dimension, the effective computation is not reduced as much as the locally linear embedding method should offer. Overall, the key idea of the method therein is to seek the intersection of the hidden constitutive manifold and the equilibrium manifold by following some appropriate and adaptive search direction. The search direction is substituted into the principle of virtual work and the entire procedure is effectively iterated on the resulted equations discretized by the finite element method.

It is beneficial to acknowledge the works that have embedded the data-based approaches into computational mechanics. The so-called neural network constitutive model is introduced and implemented in the work by Hashash et al. [18]. To put it simply, the neural networks could be interpreted as an approximation tool that calibrates the constitutive law represented by an approximate functional relationship. The most crucial contribution of this work is the derivation of the material stiffness matrix from the neural network constitutive models, which is pertinent to any finite-element-based solvers. The robustness and reliability of the proposed material model were demonstrated on several boundary value problems. Due to the lack of experiments, the training sets for the neural network constitutive models were produced in virtual of the existing models. Built upon this work, Zopf and Kaliske [19] have recently combined the neural network technique with the micro-sphere model that was developed in the work of Miehe et al. [20] in order to study the model-free

[1] This undesirable property is not inherent in the updated Lagrangian Hencky formulation which is a total formulation itself.

characterization of elastic and inelastic materials. Keeping in mind that the strain-stress experimental data can be hardly extracted in the three-dimensional environment without advanced measurement techniques, this combination assists the neural network material model to represent the general material behavior based on one-dimensional material data. As for application they conducted a set of standard uniaxial compression and tensile tests on uncured elastomers using either single stage or cyclic loading. In addition, relaxation and plastic response tests were carried out. The collected data was subsequently used as the input for the training process and the model-free material characterization proves to be quite robust and promising. As the utmost validation the model-free characterization was implemented into a finite element software and the simulation of a complex forming of a rubber block into a mould produced reliable results.

The neural network approach is distinguishable from the distance-minimizing data-driven computing in the following sense. While the former constructs the constitutive law before any solution procedure is applied, the latter incorporates this construction into the mathematical model as a complete entity. It is worthwhile to compare the distance-minimizing approach to the work by Ibrahimbegovic et al. [21] regarding the optimal design and optimal control. The design variables are introduced into an objective function or a cost function while the physical constraint, namely the principle of virtual work, is enforced by the use of a Lagrange multiplier. Then the evolution-based strategies are used to solve the global optimization problem. The optimal solution yields the optimal design as well as the optimal control variables. Nevertheless, we cannot make the spirits of the current work and the above-mentioned work identical due to the nature of the problems at hand. Keeping in mind that our ultimate aim is to solve the boundary value problems of continuum mechanics by using only material data, we must not be ignorant of the physical instability points introduced into the model by geometrical nonlinearity. Indeed, it is not guaranteed that a global optimal solution can be obtained in nonlinear problems during a loading process.

The contribution of the present work is to extend the idea of Kirchdoerfer and Ortiz [16] to large deformations. In doing so, we try to give additional insights into the method and interpret the data-driven algorithm as the steepest descent method. To this end, we present consistently the derivation and the numerical computation so that the typical flowchart of a data-driven model can be exposed. The formulation is derived first for one-dimensional continuum elements and then extended to the two-dimensional case. As for validation of the proposed scheme, several convergence studies are performed and the problems are deliberately constructed so that the reference solutions are either extracted from reliable mathematical software or exact solutions. The general convergence issue has been analyzed in the work [16].

2. Data-driven solver for bar with variable cross-sectional area

We start with considering a simple problem of a one-dimensional bar with variable cross-sectional area. The configuration of this first example is depicted in Fig. 1. For illustration we examine the elasticity problem within the finite strain theory.

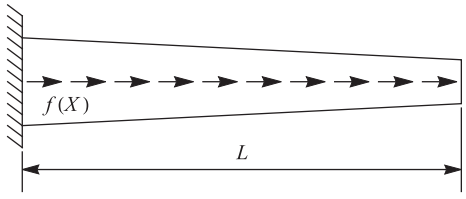

Fig. 1. Simple bar with variable cross-sectional area.

2.1. Formulation of the optimization problem

The material behavior of the bar can be characterized by a simple relation between the axial strain and the resultant axial stress. Upon suggestion of [16], the space Z containing the generic pairs of strain-stress is referred to as *phase space*. Instead of the functional relationship $\boldsymbol{\sigma} = \boldsymbol{\sigma}(\boldsymbol{\epsilon})$, we are provided with a set of material data which can be listed as $(\boldsymbol{\epsilon}_m, \boldsymbol{\sigma}_m)$, $m = 1, \dots, M$, so the list $\{(\boldsymbol{\epsilon}_m, \boldsymbol{\sigma}_m)\}_{m=1}^{M}$ is a discrete finite subset of Z. In this notation $\boldsymbol{\epsilon}$ and $\boldsymbol{\sigma}$ may imply different kinds of strain and stress measures. Typically, we may choose any strain and stress measures in either reference configuration or current configuration. In this work we exclusively use the Green-Lagrange strain measure $\mathbf{E} = 1/2(\nabla_{\mathbf{X}}\mathbf{u} + \nabla_{\mathbf{X}}^{\top}\mathbf{u} + \nabla_{\mathbf{X}}\mathbf{u} \cdot \nabla_{\mathbf{X}}\mathbf{u})$, where $\mathbf{u}$ is the displacement vector of a material particle labeled by the reference coordinate $\mathbf{X}$, and the second Piola-Kirchhoff stress tensor $\mathbf{S}$ which are known to provide objective equations of state. For the one-dimensional case they reduce to the scalar strain E and the scalar stress S. We assume that the bar is homogeneous so that the same material data can be used for the entire bar. Nevertheless, we shall not discuss where and how these experimental data can be extracted but only point out that they can be collected either in the laboratory or from the experimental-based simulations (Kalidindi et al. [23], Agarwal and Dhar [24]). Instead, the focus of the present work is to recognize the mathematical structure we are dealing with.

Basically, the classical strain and stress fields are treated as continuous tensor-valued functions on some domain of interest Ω in a continuum body. In principle we may abstract the given strain-stress data as a mapping from the domain Ω to the range of provided data values. Thus this mapping has the same definition domain as that for the classical strain and stress but its range is discrete. In the classical context the strain and stress take the continuous values that are constrained to each other by a certain constitutive law. This constitutive law generates a subspace of Z, so a typical strain-stress pair in this space takes the form $(E, S(E))$. On the other hand, in the data-driven scenario this constitutive subspace is replaced with a finite discrete subset of Z (cf. [16]). So a typical pair $(E, S(E))$ is now replaced with one of the possibilities (E_m, S_m). We denote such a set of functions by $\mathcal{E}$ and its description is visualized in Fig. 2.

In the subsequent discussion the term "element" is put in the context of finite element method. In the first attempt of investigation let us consider a bar consisting of only one element. The bar is subject to the distributed uniaxial force per unit volume $f(X)$, where X is the coordinate of a material point in the reference configuration. Under the kinematic assumptions of a structural bar element, the actual displacement $u(X)$ is governed by the principle of virtual work

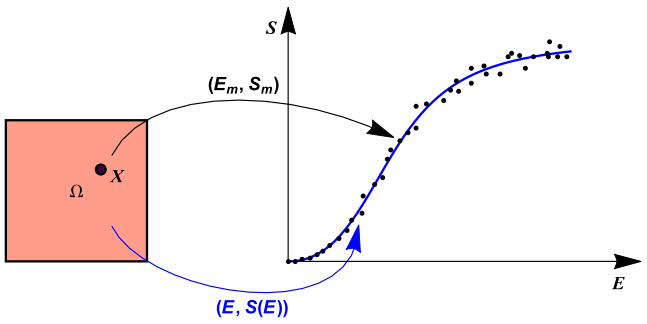

Fig. 2. Visualization of strain and stress fields in the data-driven context.

$$\int_0^L S(X)\delta E(X)A(X)\mathrm{d}X = \int_0^L f(X)\delta u(X)A(X)\mathrm{d}X, \tag{1}$$

where the one-dimensional Green-Lagrange strain is given by

$$E = \frac{\mathrm{d}u}{\mathrm{d}X} + \frac{1}{2}\left(\frac{\mathrm{d}u}{\mathrm{d}X}\right)^2. \tag{2}$$

and the differential volume element $\mathrm{d}V = A\mathrm{d}X$ has been used. Since the functional relationship $S = S(E)$ is not available, we cannot cast this variational formulation to the standard displacement-driven formulation. Based on the previous work [16], we start with the penalty function

$$F(E,S) = \min_{(E',S')\in\mathcal{E}} \int_V C(E-E')^2\mathrm{d}V + \int_V \frac{1}{C}(S-S')^2\mathrm{d}V, \tag{3}$$

where $\mathcal{E}$ is the subset of Z described above, $C = C(X)$ is a positive function, and V is the volume of the bar. If we are at the current point $\mathbf{z} = (E,S) \in Z$, this penalty function equips a distance measure from $\mathbf{z}$ to the subset $\mathcal{E} \subset Z$. There are two remarks on this definition. Firstly, it is clear that the optimization problem contained in (3) has the optimal solution making the functional F well-defined. The functions in subset $\mathcal{E}$ only take finite number of values and thus the minimum is taken from a finite set once strain and stress fields E and S are fixed. We call the solution of this minimization problem (E^*, S^*), that is

$$\begin{aligned} F(E,S) &= \int_V C(E-E^*)^2\mathrm{d}V + \int_V \frac{1}{C}(S-S^*)^2\mathrm{d}V \\ &\leqslant \int_V C(E-E')^2\mathrm{d}V + \int_V \frac{1}{C}(S-S')^2\mathrm{d}V, \quad \forall (E',S') \in \mathcal{E}. \end{aligned}$$

Secondly, the integrals cannot be evaluated due to discrete-valued mappings E' and S', so the above integral must be modified and interpreted in a different sense. To this end, let us make use of a distributed Dirac measure and introduce the modified functional

$$F(E,S) = \int_0^L \left[w(X)C(E-E') + w(X)\frac{1}{C}(S-S')\right]A(X)\mathrm{d}X,$$

where $w(X)$ is the linear combination of Dirac delta functions characterized by a mesh of collocation points $\{X_g\}_{g=1}^{N_g}$ and the corresponding weights $\{w_g\}_{g=1}^{N_g}$, that is

$$w(X) = \sum_{g=1}^{N_g} w_g \delta(X - X_g). \tag{4}$$

Substituting this weight function into the integral, F can be explicitly written as follows:

$$F(E,S) = \sum_{g=1}^{N_g} w_g C_g \left[E_g - E_g^*\right]^2 A_g + \sum_{g=1}^{N_g} w_g C_g \left[S_g - S_g^*\right]^2 A_g, \tag{5}$$

where $E_g = E(X_g)$, $E_g^* = E^*(X_g)$, $S_g = S(X_g)$, $S_g^* = S^*(X_g)$, $C_g = C(X_g)$ and $A_g = A(X_g)$.

Relating to the physical problem at hand, we must enforce the conservation law (1) and the strain definition (2). Generally, the compatibility condition on the displacement is automatically satisfied by proper use of basis functions and correct imposition of essential boundary conditions (see also Bathe [25]). For that reason, we prefer not to address (2) as the compatibility condition (cf. [16]). The second constraint gives us the possibility to implement the kinematics of physical problems such as the essential boundary conditions and it can be easily enforced by direct substitution in F. Consequently, we arrive at the following minimization problem

- Objective function:

$$F(E,S) \longrightarrow \min_{(E,S)\in\mathcal{E}} \tag{6}$$

- Constraints:

$$\begin{aligned} &\int_0^L w_p(X)S(X)\delta E(X)A(X)\mathrm{d}X = \int_0^L w_p(X)f(X)\delta u(X)A(X)\mathrm{d}X, \quad \forall \delta u \in H_0^1(\Omega), \\ &E = \frac{\mathrm{d}u}{\mathrm{d}X} + \frac{1}{2}\left(\frac{\mathrm{d}u}{\mathrm{d}X}\right)^2, \end{aligned} \tag{7}$$

in which the weight function w_p has been associated with the principle of virtual work. The latter corresponds to the weighted Galerkin method. Here we also use the notation $H_0^1(\Omega)$, with $\Omega = [0,L]$, for the Sobolev space of functions that vanish only at the left boundary, that is

$$H_0^1(\Omega) = \left\{ v \in H^1(\Omega) \,|\, v(X=0) = 0 \right\}.$$

We notice that the weighted conservation law $(7)_2$ cannot be considered as a standard constraint in a typical optimization problem as it would give out an infinite number of equality constraints, each corresponding to one choice of virtual displacement. Although one can use the notion of Lagrange multiplier on the Banach space, it is sufficient in our first attempt to consider the finite element formulation on a finite-dimensional space. In that case, scalar Lagrange multipliers can be employed. Furthermore, the concentrated load can be easily incorporated in the formulation by adding a Dirac delta function to $f(X)$. It will be recognized in the subsequent considerations that the externally applied loads can be computed by following the standard finite element procedure. As the boundary terms involving the natural boundary conditions do not interfere the derivation, we conceive that these boundary terms can be dealt with in the standard procedure and thus are not addressed in our discussion.

We solve the approximate problem of $(7)_2$ as follows: Find $S \in L^2(\Omega)$ such that

$$\int_0^L w_p S\left[\frac{\mathrm{d}\delta u}{\mathrm{d}X} + \frac{\mathrm{d}u}{\mathrm{d}X}\frac{\mathrm{d}\delta u}{\mathrm{d}X}\right]A\mathrm{d}X = \int_0^L w_p f \delta u A\mathrm{d}X, \quad \forall \delta u \in V_0(\Omega),$$

where $V_0^1(\Omega)$ is the finite element space defined as[2]

$$V_0^1(\Omega) = \left\langle \phi_j, \quad j = 1,\ldots,N \,|\, \phi_j(0) = 0, \quad \phi_j \in H^1(\Omega) \right\rangle.$$

At this step we do not specify the finite-dimensional space for S but leave it general for convenience of further development. This approximate problem is now engendered to a finite number of equations

$$\int_0^L w_p S\left[\frac{\mathrm{d}\phi_j}{\mathrm{d}X} + \frac{\mathrm{d}u}{\mathrm{d}X}\frac{\mathrm{d}\phi_j}{\mathrm{d}X}\right]A\mathrm{d}X = \int_0^L w_p f \phi_j A\mathrm{d}X, \quad j = 1,\ldots N.$$

Now it is possible to enforce this set of constraints by the method of Lagrange multipliers. We search for the solution u of the optimization problem (6) and (7) in the same functional space $V_0^1(\Omega)$. That is, the solution u is interpolated by

$$u = \sum_{i=1}^{N} \phi_i u_i = \boldsymbol{\Phi}\mathbf{u},$$

where

$$\boldsymbol{\Phi} = [\,\phi_1 \quad \ldots \quad \phi_N\,], \quad \mathbf{u} = [\,u_1 \quad \ldots \quad u_N\,]^\top.$$

[2] A short reference of Sobolev spaces for the finite element method can be found in the long-standing book by Johnson [28].

Introducing the Lagrange multipliers η_j, $j = 1, \dots, N$, assembled in the column vector $\boldsymbol{\eta}$, we have just obtained the effective objective function

$$\Pi(\mathbf{u}, S, \boldsymbol{\eta}) = \sum_{g=1}^{N_g} w_g \left[\frac{1}{2} C_g (E_g(\mathbf{u}) - E_g^*)^2 + \frac{1}{2C_g} (S_g - S_g^*)^2 \right] A_g - \sum_{j=1}^{N} \eta_j \left\{ \int_0^L w_p S \left[\frac{\mathrm{d}\phi_j}{\mathrm{d}X} + \frac{\mathrm{d}u}{\mathrm{d}X} \frac{\mathrm{d}\phi_j}{\mathrm{d}X} \right] A \mathrm{d}X - \int_0^L w_p f \phi_j A \mathrm{d}X \right\}, \tag{8}$$

where

$$E_g(\mathbf{u}) = \sum_{j=1}^{N} u_j \frac{\mathrm{d}\phi_j}{\mathrm{d}X}(X_g) + \frac{1}{2} \sum_{i=1}^{N} \sum_{j=1}^{N} \frac{\mathrm{d}\phi_i}{\mathrm{d}X}(X_g) \frac{\mathrm{d}\phi_j}{\mathrm{d}X}(X_g) u_i u_j.$$

Before moving on, we summarize the essential ingredients in our formulation and discuss some potential issues. In order to obtain the effective objective function, we need to combine the penalty function with the physical constraint, namely the principle of virtual work, through the use of a Lagrange multiplier. While the physical constraint remains unchanged in the mathematical formulation, the choice of the penalty function depends on in which form we intend to incorporate the given data in our formulation. For instance, instead of using the Green-Lagrange strain paired with the second Piola-Kirchhoff stress (which are independent of rotation of the observation frame), one could extract different kinds of deformation and stress measures from existing data (which may, for example, be at hand in terms of displacement gradient and first Piola-Kirchhoff stress). For that reason, we emphasize that the derivation of the mathematical formulation in this work can in principle be applied to other treatments of existing data by adjusting the penalty function. The main motivation for our choice of pairing the second Piola-Kirchhoff stress and the Green-Lagrange strain is (i) to have a penalty function that is automatically objective, and (ii) to relate our work closely to the existing results of [16].

The parameter C in (3) plays the role of weighting the units of the strain and the stress so that their intrinsically physical values do not dominate each other. We find that a suitable choice of C would be in the order of the norm of the material constitutive matrix that is usually derived from the classical constitutive law. Such order can be numerically achieved by using the idea of locally linear tangent surface that could be constructed by minimizing the following function with respect to C and C_0

$$\mathcal{T}(C, C_0) = \sum_{i \in \mathcal{N}(K, \mathbf{z})} (S_i - C E_i - C_0)^2,$$

where $\mathcal{N}(K, \mathbf{z})$ is the set of K-nearest-neighbors of a generic point $\mathbf{z} = (E, S) \in Z$. We refer to the work by Ibañez et al. [17] and Roweis and Saul [27] for the method of locally linear embedding. In this particular situation we only borrow the idea but do not really perform the operation of model order reduction.

It is not imperative to estimate all values C_g beforehand, one common value also works. But it is more important that we can avoid the softening effect occurring in the overall stiffness during the early stage of numerical simulation. Furthermore, it is not guaranteed that different choices of parameters C_g would lead to unique optimal solution of the effective objective function. Nevertheless, our practice dictates that deviation of these parameters in a reasonable range gives us the reliable optimal solutions, sometimes the same solutions. Discussion regarding the instabilities is delayed till the next section where the formulation for a truss system is presented.

It should be mentioned that there is no need to separate the material responses into different regimes such as elasticity, plasticity, and kinematic hardening. Yet it is obligatory to have sufficient material data in both loading and unloading conditions. The separation of data in different loading conditions is again not covered in our present work, henceforth only nonlinear elasticity is in scope. Theoretically, if the structural system is only incrementally loaded but not unloaded in the opposite direction, the data-driven solver can automatically accommodate the boundary value problems where heterogeneous strain and stress fields may occur. The work by Kucerova et al. [26] is referred for parameter identification from tests for materials characterized by three elastic, hardening and softening stages.

The next step is solve the variational equation $\delta\Pi = 0$, which leads to the application of a finite element procedure. We present in the following two approaches to the problem.

2.2. Collocation method

In the first approach we use the same weight function (4) for w_p. We note that in this manner the collocation method has just been used when specifying the weight function as Dirac delta distribution at the collocation points. In addition, if they are the Gauss points and w_g are the corresponding weight coefficients, these summations can be considered as the Gaussian quadrature of the involved integrals in the principle of virtual work (cf. Abramowitz et al. [33], Laurie [34]). Then the effective objective function (8) becomes

$$\Pi = \sum_{g=1}^{N_g} w_g \left[\frac{1}{2} C_g (E_g(\mathbf{u}) - E_g^*)^2 + \frac{1}{2C_g} (S_g - S_g^*)^2 \right] A_g - \sum_{j=1}^{N} \eta_j \left[\sum_{g=1}^{N_g} w_g S(X_g) B_{gj}(\mathbf{u}) A_g - \sum_{g=1}^{N_g} w_g f(X_g) \phi_j(X_g) A_g \right], \tag{9}$$

where

$$B_{gj}(\mathbf{u}) = \frac{\mathrm{d}\phi_j}{\mathrm{d}X}(X_g) + \sum_{i=1}^{N} u_i \frac{\mathrm{d}\phi_i}{\mathrm{d}X}(X_g) \frac{\mathrm{d}\phi_j}{\mathrm{d}X}(X_g).$$

It is seen immediately that Π is the function of $\mathbf{u} = (u_j), \mathbf{S} = (S_g), \boldsymbol{\eta} = (\eta_j)$.

The variation of Π with respect to $\mathbf{u}, \mathbf{S}, \boldsymbol{\eta}$ degenerates to the partial differentiation of Π, that is

$$\delta\Pi = \frac{\partial \Pi}{\partial u_i} \delta u_i + \frac{\partial \Pi}{\partial S_n} \delta S_n + \frac{\partial \Pi}{\partial \eta_i} \delta \eta_i,$$

in which we have used the Einstein summation convention. Invoking the variational equation $\delta\Pi = 0$, the following set of equations can be derived

$$\begin{aligned} 0 &= \frac{\partial \Pi}{\partial u_i} = \sum_{g=1}^{N_g} w_g C_g (E_g(\mathbf{u}) - E_g^*) \frac{\partial E_g}{\partial u_i}(\mathbf{u}) A_g - \sum_{j=1}^{N} \eta_j \sum_{g=1}^{N_g} w_g S_g \frac{\partial B_{gj}}{\partial u_i}(\mathbf{u}) A_g, \\ 0 &= \frac{\partial \Pi}{\partial S_n} = w_n \frac{1}{C_n} (S_n - S_n^*) A_n - \sum_{j=1}^{N} \eta_j w_n B_{nj}(\mathbf{u}) A_n, \\ 0 &= \frac{\partial \Pi}{\partial \eta_i} = - \left[\sum_{g=1}^{N_g} w_g S_g B_{gi}(\mathbf{u}) A_g - \sum_{g=1}^{N_g} w_g f(X_g) \phi_i(X_g) A_g \right]. \end{aligned} \tag{10}$$

The last equation corresponds to the equality constraints or the principle of virtual work in the finite-dimensional functional space. By denoting

$$H_{ij} = \frac{\mathrm{d}\phi_i}{\mathrm{d}X}\frac{\mathrm{d}\phi_j}{\mathrm{d}X},$$

it is straightforward to verify that

$$\frac{\partial E_g}{\partial u_i} = \frac{\mathrm{d}\phi_i}{\mathrm{d}X}(X_g) + \sum_{j=1}^{N} u_j H_{ji}(X_g) = B_{gi}(\mathbf{u}),$$
$$\frac{\partial B_{gj}}{\partial u_i}(\mathbf{u}) = \frac{\mathrm{d}\phi_i}{\mathrm{d}X}(X_g)\frac{\mathrm{d}\phi_j}{\mathrm{d}X}(X_g) = H_{ij}(X_g). \tag{11}$$

We can eliminate S_g from the system by using the second equation (12) in the form

$$S_g = \sum_{j=1}^{N} C_g B_{gj}(\mathbf{u})\eta_j + S_g^* \tag{12}$$

to obtain the system

$$\sum_{g=1}^{N_g} w_g C_g \left[E_g(\mathbf{u}) - E_g^*\right] B_{gi}(\mathbf{u}) A_g - \sum_{j=1}^{N}\left[\sum_{g=1}^{N_g} w_g S_g(\mathbf{u},\boldsymbol{\eta}) H_{ij}(X_g) A_g\right]\eta_j = 0,$$

$$\sum_{g=1}^{N_g} w_g S_g(\mathbf{u},\boldsymbol{\eta}) B_{gi}(\mathbf{u}) A_g - \sum_{g=1}^{N_g} w_g f(X_g)\phi_i(X_g) A_g = 0, \quad i = 1,\dots,N,$$

where we have signified that S_g depends on $\mathbf{u}$ and $\boldsymbol{\eta}$.

This system of equations can be solved by the Newton-Raphson method. To this end, we rewrite it as follows

$$[P_u]_i := \sum_{g=1}^{N_g} w_g A_g C_g \left[E_g(\mathbf{u}) B_{gi}(\mathbf{u}) - E_g^*[B_1(\mathbf{u})]_{gi}\right] - \sum_{j=1}^{N}\sum_{g=1}^{N_g} w_g A_g S_g(\mathbf{u},\boldsymbol{\eta}) H_{ij}(X_g)\eta_j = \sum_{g=1}^{N_g} w_g A_g C_g E_g^* \frac{\mathrm{d}\phi_i}{\mathrm{d}X}(X_g) =: [F_{E^*}]_i,$$

$$[P_\eta]_i := \sum_{g=1}^{N_g} w_g A_g S_g(\mathbf{u},\boldsymbol{\eta}) B_{gi}(\mathbf{u}) = \sum_{g=1}^{N_g} w_g A_g f(X_g)\phi_i(X_g) =: f_i,$$

where

$$[B_1(\mathbf{u})]_{gi} = \sum_{j=1}^{N} u_j H_{ji}(X_g). \tag{13}$$

Then the tangent stiffness is given by

$$\mathbf{K} = \begin{bmatrix} \dfrac{\partial \mathbf{P_u}}{\partial \mathbf{u}} & \dfrac{\partial \mathbf{P_u}}{\partial \boldsymbol{\eta}} \\ \dfrac{\partial \mathbf{P_\eta}}{\partial \mathbf{u}} & \dfrac{\partial \mathbf{P_\eta}}{\partial \boldsymbol{\eta}} \end{bmatrix}.$$

We recall that in the finite element procedure a similar structure of the tangent stiffness matrix can be found in various structural and continuum elements. The difference lies in the assumptions on the kinematics of elements under consideration. A good summary upon the present discussion is given in the textbook by Bathe (Section 4.2.1 in [25]). Hence, it is instructive to derive the tangent stiffness matrix in more detail as it happens that the similar computation can be carried out in the subsequent sections. We compute the partial derivatives

$$\frac{\partial [P_u]_i}{\partial u_j} = \sum_{g=1}^{N_g} w_g A_g C_g \left[\frac{\partial E_g}{\partial u_j} B_{gi}(\mathbf{u}) + E_g(\mathbf{u})\frac{\partial B_{gi}}{\partial u_j} - E_g^*\frac{\partial [B_1(\mathbf{u})]_{gi}}{\partial u_j}\right] - \sum_{k=1}^{N} w_g A_g \frac{\partial S_g}{\partial u_j} H_{ik}\eta_k,$$

$$\frac{\partial [P_u]_i}{\partial \eta_j} = -\sum_{k=1}^{N}\sum_{g=1}^{N_g} w_g A_g \left[S_g H_{ik}(X_g)\delta_{jk} + \frac{\partial S_g}{\partial \eta_j} H_{ik}(X_g)\eta_k\right],$$

$$\frac{\partial [P_\eta]_i}{\partial u_j} = \sum_{g=1}^{N_g} w_g A_g \left[S_g \frac{\partial B_{gi}}{\partial u_j} + \frac{\partial S_g}{\partial u_j} B_{gi}(\mathbf{u})\right],$$

$$\frac{\partial [P_\eta]_i}{\partial \eta_j} = \sum_{g=1}^{N_g} w_g A_g \frac{\partial S_g}{\partial \eta_j} B_{gi}(\mathbf{u}).$$

It follows by differentiating Eqs. (12) and (13) that

$$\frac{\partial S_g}{\partial u_j} = \sum_{i=1}^{N} C_g H_{ji}(X_g)\eta_i, \quad \frac{\partial S_g}{\partial \eta_j} = C_g B_{gj}(\mathbf{u}), \quad \frac{[B_1(\mathbf{u})]_{gi}}{\partial u_j} = H_{ji}(X_g). \tag{14}$$

Substituting (11) and (14) into the above expressions, we obtain the following tangent stiffness in the indicial notation

$$\frac{\partial [P_u]_i}{\partial u_j} = \sum_{g=1}^{N_g} w_g A_g C_g \left\{B_{gi}(\mathbf{u}) B_{gj}(\mathbf{u}) + (E_g(\mathbf{u}) - E_g^*) H_{ij}(X_g) - [B_1(\boldsymbol{\eta})]_{gi}[B_1(\boldsymbol{\eta})]_{gj}\right\},$$

$$\frac{\partial [P_u]_i}{\partial \eta_j} = -\sum_{g=1}^{N_g} w_g A_g \left\{C_g [B_1(\boldsymbol{\eta})]_{gi} B_{gj}(\mathbf{u}) + S_g(\mathbf{u},\boldsymbol{\eta}) H_{ij}(X_g)\right\},$$

$$\frac{\partial [P_\eta]_i}{\partial u_j} = \sum_{g=1}^{N_g} w_g A_g \left\{C_g B_{gi}(\mathbf{u})[B_1(\boldsymbol{\eta})]_{gj} + S_g(\mathbf{u},\boldsymbol{\eta}) H_{ji}(X_g)\right\},$$

$$\frac{\partial [P_\eta]_i}{\eta_j} = \sum_{g=1}^{N_g} w_g A_g C_g B_{gi}(\mathbf{u}) B_{gj}(\mathbf{u}),$$

where we have reused definition (13) with $\boldsymbol{\eta}$ being in replacement of $\mathbf{u}$, that is

$$[B_1(\boldsymbol{\eta})]_{gi} = \sum_{j=1}^{N} \eta_j H_{ji}(X_g).$$

The incremental solution is achieved through the following iterative process

$$\mathbf{K}(\mathbf{q}^{(i)})\Delta\mathbf{q}^{(i)} = \begin{bmatrix} \mathbf{F}_{E^*} \\ \mathbf{f} \end{bmatrix} - \begin{bmatrix} \mathbf{P_u} \\ \mathbf{P_\eta} \end{bmatrix}(\mathbf{q}^{(i)}), \quad \mathbf{q}^{(i+1)} = \mathbf{q}^{(i)} + \Delta\mathbf{q}^{(i)}, \quad \text{where} \quad \mathbf{q} = \begin{bmatrix} \mathbf{u} \\ \boldsymbol{\eta} \end{bmatrix}. \tag{15}$$

There are some important practices in solving system (15) iteratively. First, the externally applied force can be controlled by adding an incremental force step by step. Thus, it is possible to apply nonproportional loading or cyclic loading. The entire scheme remains unchanged except that the force vector $\mathbf{f}$ in (15) must be replaced by the force vector at a specific step. The simulations in the present work are conducted by controlling the force as follows

$$\mathbf{f}_a = \left(\sum_{b=1}^{a}\mu_b\right)\left(\sum_{b=1}^{N_f}\mu_b\right)^{-1}\mathbf{f}, \quad \mu_b > 0, \quad a = 1,\dots,N_f, \quad \mathbf{f}_{N_f} = \mathbf{f},$$

where N_f is the total number of load steps. Second, as for the stopping criterion we choose

$$\frac{\|\mathbf{F} - \mathbf{P}\|}{\|\mathbf{F}\|} < \mathrm{TOL}, \quad \text{where} \quad \mathbf{F} = \begin{bmatrix} \mathbf{F}_{E^*} \\ \mathbf{f} \end{bmatrix}, \quad \mathbf{P} = \begin{bmatrix} \mathbf{P_u} \\ \mathbf{P_\eta} \end{bmatrix}$$

and the norm is defined by $\|\mathbf{a}\| = \left(\sum_i a_i^2\right)^{1/2}$. The tolerance (TOL) should be small enough so that the accuracy is not influenced by the density of the material data. If distances between two nearest

data points have the mean value of order $O(10^{-n})$, the tolerance should have the smaller order, say $O(10^{-m})$, where $m > n$. In fact, it is rather easy to satisfy this requirement because the distances between the data points from experiments are usually much larger than the usual tolerance used in the Newton-Raphson method. We choose $\mathrm{TOL} = 10^{-6}$ in our numerical simulations and the convergence studies below demonstrate that it is sufficient. Last but not least, a modified Newton-Raphson method is used in that the tangent stiffness is kept unchanged for each increment load. It is aimed to reduce the computational cost in the assembly process and also to preserve convergence rate of the Newton-Raphson method to some extent (see for example [25]).

We make one further remark here. If a constant cross-sectional area and a linearized strain measure are assumed, the effective objective function is exactly the same as that given in [16], which can be explained as follows. The "physical" Gauss-Legendre quadrature pairs $\{(w_g, X_g)\}_{g=1}^{N_g}$ are related to the reference ones $\{(w_g^r, X_g^r)\}_{g=1}^{N_g}$, which are defined on the reference interval $[-1, 1]$, by

$$w_g = w_g^r \frac{L}{2}, \quad X_g = (1 + X_g^r)\frac{L}{2}.$$

Recalling that the sum of Gaussian quadrature weights w_g^r is equal to two (cf. Stoer [35]), we have

$$\sum_{g=1}^{N_g} w_g A_g = A\frac{L}{2}\sum_{g=1}^{N_g} w_g^r = A \times L,$$

which is the volume of the bar element. In addition, the B-matrix does not depend on the displacements, the strain E_g degenerates to ϵ_g which is linearly dependent on the displacements, the stress S_g degenerates to the engineering stress σ_g and also $H_{ij} = 0$. In such a circumstance the tangent stiffness reduces to the stiffness matrix obtained in [16], that is

$$\frac{\partial [P_u]_i}{\partial u_j} = \sum_{g=1}^{N_g} V_g C_g B_{gi} B_{gj}, \quad \frac{\partial [P_\eta]_i}{\partial \eta_j} = \sum_{g=1}^{N_g} V_g C_g B_{gi} B_{gj}, \quad \frac{\partial [P_u]_i}{\partial \eta_j} = \frac{\partial [P_\eta]_i}{\partial u_j} = 0.$$

Moreover, when one wishes to discretize the bar into several small elements, approximately assumes constant cross-sectional area for each element and use the quadrature Gauss points within the individual elements, the weights in the objective function will automatically become the volumes of those elements. Further discussion regarding the weight factors w_g will be addressed in the next section.

It is valuable to notice further that the present approach is comparable to the displacement/pressure formulation. Particularly, the above discussion bears resemblance to the displace ment/pressure-formulation which in turn belongs to the class of mixed finite element formulations (cf. Section 4.4.3 in Bathe [25] and Brezzi [29]). Consequently, one might expect that locking phenomena may not create much concern. Furthermore, as the stresses evaluated at the Gauss points pertain only to the element, the use of the static condensation at the element level is possible. This practice was used in the preceding derivation when the stresses at the Gauss points are eliminated from the system.

2.3. Interpolation method

By using the collocation method as above, we have implicitly dealt with the familiar finite element method when a sufficient number of Gauss points in the quadrature integration is used. Indeed, the principle of virtual work is computed in practice by using the numerical quadrature and the actual implementation is what we have presented (cf. [25]). One can actually keep $w_p = 1$ and approximate the finite element equations by using the numerical integration formula as in the finite element method and then employ it as the equilibrium constraint. Then the same result is achieved. However, we have ignored a possibility that the stress field can be interpolated in a finite-dimensional subspace of $L^2(\Omega)$. For that we have more choices and thus more degrees of freedom corresponding to the stress field rather than its value at the Gauss points. When one uses the polynomial interpolation for the displacement-driven finite element formulation, it is natural to use the stress values at the Gauss points as it is proved that at these points the strain and stress fields converge at higher rate than at the others (Douglas and Dupont [30], Wahlbin and Oden [31]). This superconvergence property turns out very helpful in the posteriori analysis of the finite element solution (see for example Ainsworth [32]). But once interpolations other than polynomials are in use, this property could be violated. Taking into account the freedom of interpolating the stress field and selecting collocation points rather than the Gauss points, we can scope different kinds of finite elements in the future.

We reuse the penalty function (5) but modify the set of constraints as follows

$$\int_0^L S(X)\left(1 + \frac{\mathrm{d}u}{\mathrm{d}X}\right)\frac{\mathrm{d}\phi_j}{\mathrm{d}X}A(X)\mathrm{d}X = \int_0^L f(X)\phi_j(X)A(X)\mathrm{d}X, \quad \forall j = 1, \ldots, N.$$

Then we look for the solution $S(X)$ in the finite-dimensional functional space

$$W(\Omega) = \left\langle \psi_k, k = 1, \ldots, N_S \,|\, \psi_k \in L^2(\Omega) \right\rangle.$$

Thus, the effective objective function is now modified to

$$\Pi(\mathbf{u}, \mathbf{S}, \boldsymbol{\eta}) = \sum_{g=1}^{N_g} w_g \left[\frac{1}{2}C_g\left(E_g(\mathbf{u}) - E_g^*\right)^2 + \frac{1}{2C_g}(S_g - S_g^*)^2\right]A_g - \sum_{j=1}^{N}\eta_j\left[\int_0^L\left(\sum_{k=1}^{N_S} S_k\psi_k\right)\left(1 + \frac{\mathrm{d}u}{\mathrm{d}X}\right)\frac{\mathrm{d}\phi_j}{\mathrm{d}X}A(X)\mathrm{d}X - \int_0^L f(x)\phi_j(X)A(X)\mathrm{d}X\right],$$

where $\mathbf{S} = (S_k)$ collects the stress degrees of freedom. Invoking the variational equation (the Einstein summation convention is assumed)

$$\delta\Pi = \frac{\partial\Pi}{\partial u_i}\delta u_i + \frac{\partial\Pi}{\partial S_n}\delta S_n + \frac{\partial\Pi}{\partial \eta_i}\delta\eta_i = 0,$$

the following set of equations is obtained.

- For $\partial\Pi/\partial u_i = 0$:

$$\sum_{g=1}^{N_g} w_g A_g C_g\left\{E_g(\mathbf{u})B_{gi}(\mathbf{u}) - E_g^*[B_1(\mathbf{u})]_{gi}\right\} - \sum_{j=1}^{N}\eta_j\left[\sum_{k=1}^{N_S}\int_0^L \psi_k\frac{\mathrm{d}\phi_i}{\mathrm{d}X}\frac{\mathrm{d}\phi_j}{\mathrm{d}X}A(X)\mathrm{d}X\right]S_k = \sum_{g=1}^{N_g} w_g A_g C_g E_g^*\frac{\mathrm{d}\phi_i}{\mathrm{d}X}(X_g).$$

- For $\partial\Pi/\partial S_n = 0$:

$$\sum_{k=1}^{N_S}\left[w_g A_g \frac{1}{C_g}\psi_n(X_g)\psi_k(X_g)\right]S_k - \sum_{j=1}^{N}\eta_j\left[\int_0^L \psi_n \frac{\mathrm{d}\phi_j}{\mathrm{d}X}\left(1+\frac{\mathrm{d}u}{\mathrm{d}X}\right)A(X)\mathrm{d}X\right] = \sum_{g=1}^{N_g} w_g A_g \frac{1}{C_g} S_g^* \psi_n(X_g).$$

- For $\partial\Pi/\partial\eta_i = 0$:

$$\sum_{k=1}^{N_S}\left[\int_0^L \psi_k\left(1+\frac{\mathrm{d}u}{\mathrm{d}X}\right)\frac{\mathrm{d}\phi_i}{\mathrm{d}X}A(X)\mathrm{d}X\right]S_k = \int_0^L f(X)\phi_i(X)A(X)\mathrm{d}X.$$

We cannot use the static condensation at the element level in this approach as the stress field is continuous throughout the nodal degrees of freedom and hence an assemblage of all elements is needed. We denote the left-hand sides of the above equations as $\mathbf{P_u}$, $\mathbf{P_S}$ and $\mathbf{P_\eta}$, respectively and the right-hand sides as $\mathbf{F_{E^*}}$, $\mathbf{F_{S^*}}$ and $\mathbf{f}$, respectively. In the indicial notation, they read

$$[P_u]_i = \sum_{g=1}^{N_g} w_g A_g C_g\left\{E_g(\mathbf{u})B_{gi}(\mathbf{u}) - E_g^*[B_1(\mathbf{u})]_{gi}\right\} - \sum_{j=1}^{N}\sum_{k=1}^{N_S} a_{ijk}\eta_j S_k,$$

$$[F_{E^*}]_i = \sum_{g=1}^{N_g} w_g A_g C_g \frac{\mathrm{d}\phi_i}{\mathrm{d}X}(X_g)E_g^*,$$

$$[P_S]_n = \sum_{g=1}^{N_g}\sum_{k=1}^{N_S} w_g A_g \frac{1}{C_g}\psi_n(X_g)\psi_k(X_g)S_k - \sum_{j=1}^{N}\left[b_{nj} + \alpha_{nj}(\mathbf{u})\right],$$

$$[F_{S^*}]_n = \sum_{g=1}^{N_g} w_g A_g \frac{1}{C_g}\psi_n(X_g)S_g^*,$$

$$[P_\eta]_i = \sum_{k=1}^{N_S}[b_{ki} + \alpha_{ki}(\mathbf{u})]S_k, \quad f_i = \int_0^L f(X)\phi_i(X)A(X)\mathrm{d}X,$$

where the variables b_{nj}, a_{ijk} and α_{nj} are given by

$$b_{ni} = \int_0^L \psi_n \frac{\mathrm{d}\phi_i}{\mathrm{d}X}A(X)\mathrm{d}X, \quad a_{ijk} = \int_0^L \frac{\mathrm{d}\phi_i}{\mathrm{d}X}\frac{\mathrm{d}\phi_j}{\mathrm{d}X}\psi_k A(X)\mathrm{d}X,$$

$$\alpha_{ni}(\mathbf{d}) = \sum_{j=1}^{N} a_{ijn}d_j = \sum_{i=1}^{N} a_{jin}d_j.$$

Then the tangent stiffness appears as

$$\mathbf{K} = \begin{bmatrix} \frac{\partial \mathbf{P_u}}{\partial \mathbf{u}} & \frac{\partial \mathbf{P_u}}{\partial \mathbf{S}} & \frac{\partial \mathbf{P_u}}{\partial \boldsymbol{\eta}} \\ \frac{\partial \mathbf{P_S}}{\partial \mathbf{u}} & \frac{\partial \mathbf{P_S}}{\partial \mathbf{S}} & \frac{\partial \mathbf{P_S}}{\partial \boldsymbol{\eta}} \\ \frac{\partial \mathbf{P_\eta}}{\partial \mathbf{u}} & \frac{\partial \mathbf{P_\eta}}{\partial \mathbf{S}} & \frac{\partial \mathbf{P_\eta}}{\partial \boldsymbol{\eta}} \end{bmatrix}.$$

After some algebraic manipulation, we arrive at

$$\frac{\partial[P_u]_i}{\partial u_j} = \sum_{g=1}^{N_g} w_g A_g C_g\left[B_{gi}(\mathbf{u})B_{gj}(\mathbf{u}) + (E_g(\mathbf{u}) - E_g^*)H_{ij}(X_g)\right],$$

$$\frac{\partial[P_u]_i}{\partial S_n} = -\alpha_{ni}(\boldsymbol{\eta}), \quad \frac{\partial[P_u]_i}{\partial \eta_j} = -\sum_{k=1}^{N_s} a_{ijk}S_k, \quad \frac{\partial[P_S]_n}{\partial u_j} = -\alpha_{nj}(\boldsymbol{\eta}),$$

$$\frac{\partial[P_S]_n}{\partial S_k} = \sum_{g=1}^{N_g} w_g A_g C_g \psi_n(X_g)\psi_k(X_g), \quad \frac{\partial[P_S]_n}{\partial \eta_j} = -\left[b_{nj} + \alpha_{nj}(\mathbf{u})\right],$$

$$\frac{\partial[P_\eta]_i}{\partial u_j} = \sum_{k=1}^{N_S} a_{ijk}S_k, \quad \frac{\partial[P_\eta]_i}{\partial S_n} = b_{ni} + \alpha_{ni}(\mathbf{u}), \quad \frac{\partial[P_\eta]_i}{\partial \eta_j} = 0.$$

Similarly, the solution is attained by following the Newton-Raphson formula (14) but the solution vector $\mathbf{q}$ now collects all the degrees of freedom corresponding to the displacements, the nodal stress values and the Lagrange multipliers. We emphasize again that this formulation does not permit the static condensation at the element level. The stress interpolation does not pertain to only the individual elements but it is required that the stress must be continuous throughout the assemblage of elements. We note that this approach bears a resemblance to the u/p-c formulation (cf. [25]).

2.4. Algorithm for data-driven solver

In this subsection we summarize the algorithm for the data-driven solver that is originally suggested in the work by Kirchdoerfer and Ortiz [16]. Although one can quickly realize in this presentation that the spirit is identical, we try to comprehend the underlying arguments and to shed some light on individual steps therein. Most importantly, we conceive of the involved technique as the steepest descent method. It was emphasized in [16] that the data-driven solver is independent of the numerical method that we choose to treat the problem. Furthermore, the description herein serves as a tool for implementation of the variational formulations in the next sections.

We see that the variational equation $\delta\Pi = 0$ requires the determination of the optimal local data points (E_g^*, S_g^*) at the assemblage of collocation points. Keeping in mind that we are dealing with the discrete and finite collection of material data, the best candidates in terms of the penalty measure can be effectively sought by an iterative process. Let us assume that we are solving the optimization problem with a set of reference material data points (E_g^r, S_g^r) being known in replacement of the optimal candidates. Just like the gradient descent method, the iterative process starts with an initial guess and then seeks the next correction with the ad hoc assumption that the corrector would correspond to the right solution of the equation, or at least the better one. To this end, we may regard $(E_g^{*[k]}, S_g^{*[k]})$ is the "optimal" solution at the k-th step and then proceed to look for a better fit $(E_g^{*[k+1]}, S_g^{*[k+1]})$ in the sense it gives out the smaller penalty function value. As we have assumed that $(E_g^{*[k]}, S_g^{*[k]})$ is the optimal solution at this step, the correction of this "almost" optimal solution is obtained by invoking $\delta\Pi = 0$ and then resolving for $(E_g^{[k+1]}, S_g^{[k+1]})$.

Up to this step, we have based our arguments on the method of steepest descent (see for example Avriel [36], Synman [37]). However, since we are given only the discrete set $D = \{(E_m, S_m)\}_{m=1}^{M}$, the correction must be pulled back to the material data set D. This pull back is achieved by selecting the candidates in D that are closest to the pairs $(E_g^{[k+1]}, S_g^{[k+1]})$ in terms of the metric defined by the penalty function $F(E,S)$. Unlike the method of steepest descent in which the stop criterion is chosen such that very little effective change in the solution at the next step occurs, the stop criterion in the data-driven solver is the "exact" no effective change (compare [36,16]). This is reasonable since we are provided only with a finite collection of material data points. The entire explanation is wrapped up in Algorithm 1. The formulation that we derived above is nothing else but the solution process in the "black-box solver" boxed in this algorithm.

Algorithm 1. Algorithm for data-driven solver

Input: Data set $D = \{(E_m, S_m)\}_{m=1}^{M}$.

Geometry and mesh of the problem domain, essential boundary conditions.

Natural boundary conditions, externally applied loads.

Maximum number of iterations $N_{\max}$

Output: Displacement $\mathbf{u}$, distribution of strain $\mathbf{E}$ and stress $\mathbf{S}$.

INITIALIZATION

`% Initialize the running index`

$k = 0$.

`% Initialize sampling data assignment`

for $g = 1, \dots N_g$ **do**

  Select the initial data $(E_g^{*[0]}, S_g^{*[0]})$ at the g-th sampling point randomly from the data set D.

end

$\mathbf{E}^{*[0]} = \{E_g^{*[0]}\}_{g=1}^{N_g}, \quad \mathbf{S}^{*[0]} = \{S_g^{*[0]}\}_{g=1}^{N_g}$

DATA-DRIVEN LOOP

for $k = 1, \dots, N_{\max}$ **do**

  `% Black-box solver`

  Solve the stationary equation $\delta\Pi(\mathbf{u}, \mathbf{S}, \boldsymbol{\eta}) = 0$ for $\mathbf{u}^{[k+1]}$, $\mathbf{S}^{[k+1]}$, $\boldsymbol{\eta}^{[k+1]}$.

  Compute $E_g^{[k+1]}$, $S_g^{[k+1]}$ according to the mechanism in the `black-box solver`.

  $\mathbf{E}^{[k+1]} = \{E_g^{[k+1]}\}_{g=1}^{N_g}, \quad \mathbf{S}^{[k+1]} = \{S_g^{[k+1]}\}_{g=1}^{N_g}$.

  `% Pull-back operator/Sampling data assignment`

  Choose $(\mathbf{E}^{*[k+1]}, \mathbf{S}^{*[k+1]})$ closest to $(\mathbf{E}^{[k+1]}, \mathbf{S}^{[k+1]})$

  `% Test for convergence`

  if $\mathbf{E}^{*[k+1]} == \mathbf{E}^{*[k]}$ *and* $\mathbf{S}^{*[k+1]} == \mathbf{S}^{*[k]}$ **then**

    Stop and exit the loop.

  else

    $k \leftarrow k + 1$.

  end

end

SOLUTION ASSIGNMENT

$\mathbf{u} = \mathbf{u}^{[k]}, \quad \mathbf{E} = \mathbf{E}^{[k]}, \quad \mathbf{S} = \mathbf{S}^{[k]}$.

2.5. Sampling examples

We study the problem depicted in Fig. 1 with the applied load being given by

$$f(X) = 5\log(X + 1).$$

To illustrate the robustness of the solver, we discretize the bar as one element and employ high-order interpolations for the displacement and the stress. For the comparison purpose the conventional incompressible Mooney-Rivlin material model is used (Mooney [38], Rivlin [39]). We recall the strain energy density per unit volume

$$W(I_1, I_2) = C_1(I_1 - 3) + C_2(I_2 - 3), \quad I_3 = 1, \tag{16}$$

where C_1 and C_2 are the material constants and I_j are the invariants of the right Cauchy-Green tensor $\mathbf{C} = 2\mathbf{E} + \mathbf{I}$. The invariants I_j are defined as follows

$$I_1 = \operatorname{tr}\mathbf{C}, \quad I_2 = \frac{1}{2}\left[(\operatorname{tr}\mathbf{C})^2 - \operatorname{tr}(\mathbf{C}^2)\right], \quad I_3 = \det\mathbf{C}. \tag{17}$$

The second Piola-Kirchhoff stress tensor is related to the Green-Lagrange strain tensor via

$$S_{ij} = \frac{\partial W}{\partial E_{ij}} = 2\frac{\partial W}{\partial C_{ij}} = 2\left[\frac{\partial W}{\partial I_1}\frac{\partial I_1}{\partial C_{ij}} + \frac{\partial W}{\partial I_2}\frac{\partial I_2}{\partial C_{ij}}\right]. \tag{18}$$

For the one-dimensional response of the bar, this stress-strain relation is specialized to

$$S = 2\left[C_1(\lambda - \lambda^{-2}) + C_2(1 - \lambda^{-3})\right], \quad E = \frac{\lambda^2 - 1}{2}. \tag{19}$$

We generate material data using this material law and then add the uniformly distributed random variations to the data pairs (E_m, S_m). The variations may be understood as the slight error in the measurement process and hence the variations of small percentage

are added to the analytical strain-stress curve. The reference solution is generated by using the material law (19) and the *Mathematica* numerical solver for differential equations (Mathematica, Version 10.3 [40]). The differential form for the usage of the software is given as follows

$$\frac{\mathrm{d}}{\mathrm{d}X}\left\{A(X)S\left[\frac{\mathrm{d}u}{\mathrm{d}X}+\frac{1}{2}\left(\frac{\mathrm{d}u}{\mathrm{d}X}\right)^2\right]\left(1+\frac{\mathrm{d}u}{\mathrm{d}X}\right)\right\}+f(X)A(X)=0,$$

$$u(0)=0,\quad \frac{\mathrm{d}u}{\mathrm{d}X}(L)=0.$$

We present first the result of strain distribution obtained by using the collocation method and the interpolation method in Figs. 3 and 4, respectively. In this numerical study we use different numbers of Gauss points in the simulations which are indicated in the figures by N_g. The numerical results show excellent agreement. Next, we embed the variations in the material data and repeat the data-driven solver to produce the strain result in Fig. 5. Of course, the higher fluctuation about the analytical stress-strain curve we put in the data, the further from the reference strain solution we expect from the data-driven strain solution.

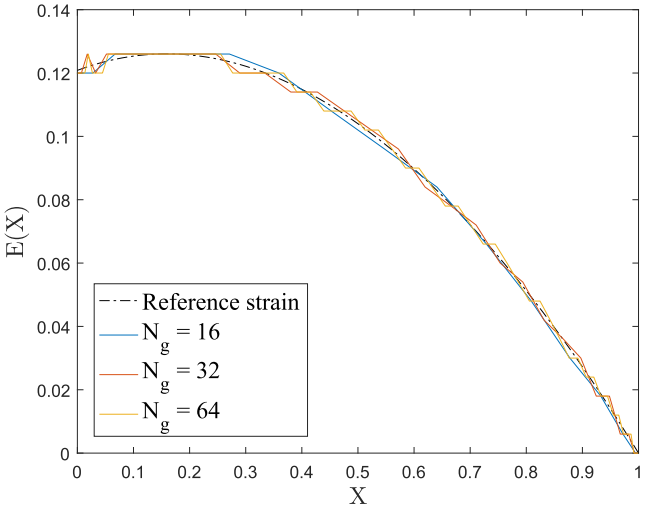

Fig. 3. Distribution of strain at the Gauss points. Solution is obtained by using the collocation method.

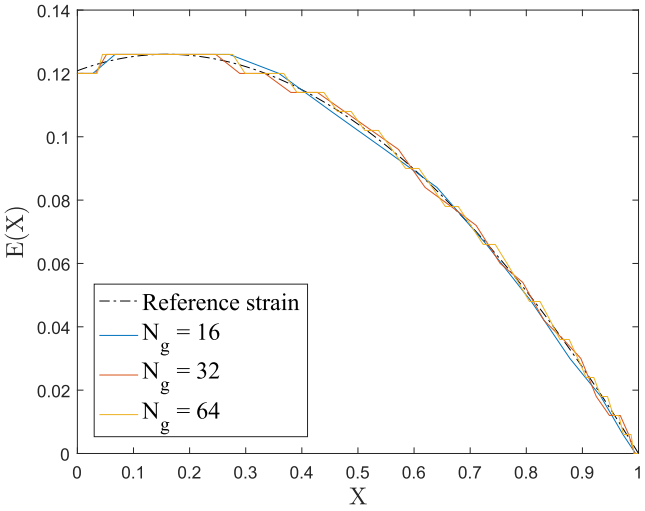

Fig. 4. Distribution of strain at the Gauss points. Solution is obtained by using the interpolation method.

Lastly, we study the convergence of the numerical solution in two regards: the convergence in regard to the size of the data and to the order of interpolation. In an equivalent approach, if we use the low-order interpolation and many finite elements, the convergence study focuses on the decrease of error with regard to the number of elements. In Fig. 6 the error in strain between data-driven and reference solutions is plotted versus the data size. The error is measured by the norm ratio

$$\frac{\|E-E^r\|}{\|E^r\|}=\frac{\left\{\sum_{g=1}^{N_g}\left[E(X_g)-E^r(X_g)\right]^2\right\}^{1/2}}{\left\{\sum_{g=1}^{N_g}\left[E^r(X_g)\right]^2\right\}^{1/2}},$$

where E^r is the reference strain solution. It should be highlighted though, that in principle the increase of data size does not necessarily assure the convergence of the data-driven solution to the finite element or analytical solution. What makes the error decrease is the higher density of strain and stress pairs around the analytical "hidden" strain and stress at the sampling points. For example, we are considering the hidden strain value E_g at a specific Gauss point. Provided that we have a large material data but the data near E_g is sparsely distributed, we have slighter chance to get closer to E_g

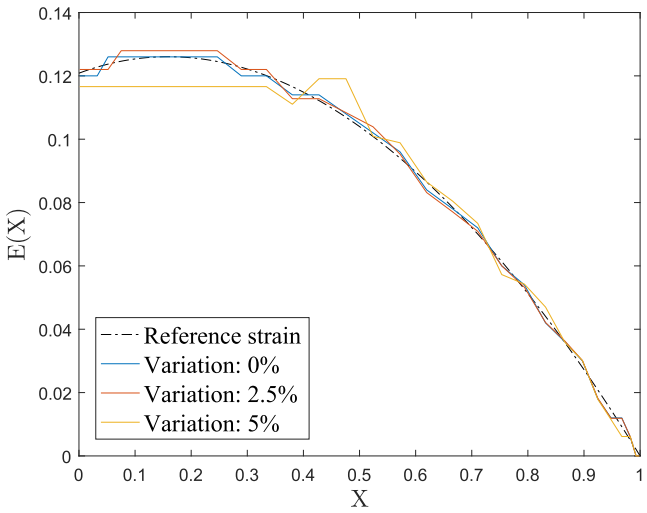

Fig. 5. Distribution of strain at the Gauss points. Solution is obtained by using the interpolation method. The data is perturbed by different variations.

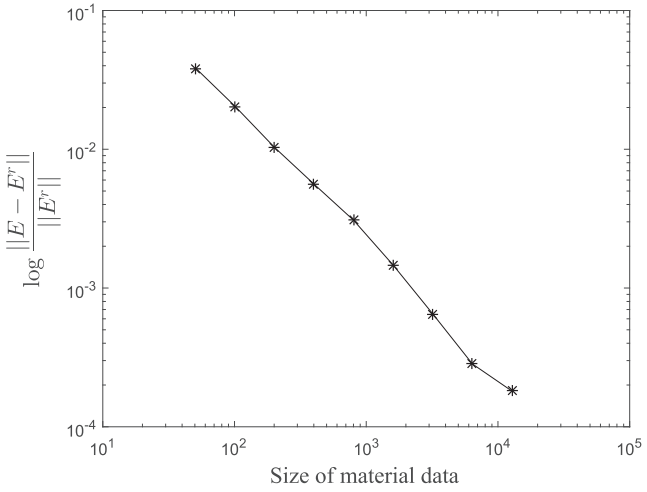

Fig. 6. Convergence of data-driven strain solution in regard to the data size.

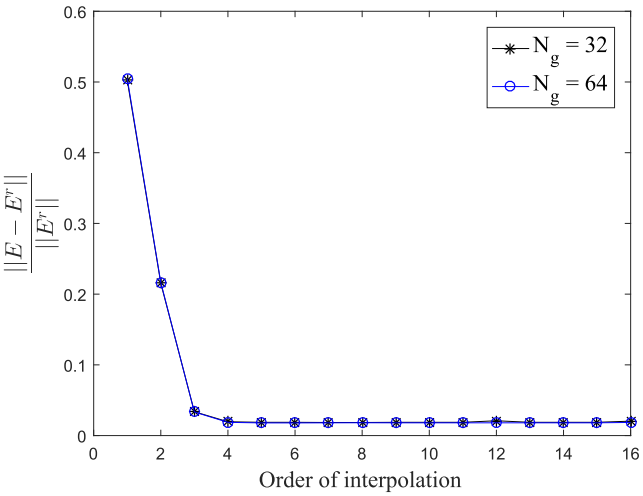

Fig. 7. Convergence of data-driven strain solution in regard to the interpolation order. Only one set of data is used in the numerical simulation, so the data size is fixed for all cases.

from such data. In an opposite scenario, if the data near E_g is densely available, then the error will be likely to be small. In the ideal case the solver might reach the "exact" hidden strain if such an exact data is available. In order to guarantee the fairness in the study of convergence with respect to the data size, a uniformly distributed data set is used in the numerical simulation. That is, the strain values are equidistant in the data set.

In Fig. 7 the result of convergence study with respect to the order of interpolation is shown. Two observations are reported from this investigation. It is clearly seen that the solution converges to the reference one with the increasing order of interpolation. However, the error metric does not decrease to zero as in the case of standard finite element solutions. In fact, the data-driven strain solution stops improving even if we assume that it is not interfered by the arithmetic error in cut-off computing process [41]. Yet it is not surprising at all as we are only allowed to select the best strain candidates from a limited data set. As the increasing order of interpolation does not help at all when the best candidates have been chosen, we should be realistic with the expectation of the order of correctness.

3. Data-driven solver for nonlinear truss structures

The data-driven solver for truss structures within the finite strain theory is developed in this section. We expect that for each truss element $e = 1, \dots, N_e$ the material data is collected in the form of pairs (E_m, S_m), $m = 1, \dots, M$.

3.1. Mathematical formulation

We assume that each truss element has constant cross-sectional area $A_0^{(e)}$ in the undeformed configuration. If there is no distributed force along any truss elements, we are examining a mathematical structural model in which the exact solution is the finite element solution itself (cf. [25]). We base our derivation on the original work [16] and the nonlinear finite element formulation for truss structures.

First the local penalty function for each bar $e = 1, \dots, N_e$ is defined by[3]

$$F_e(E^{(e)}, S^{(e)}) = \min_{(E^{(e)\prime}, S^{(e)\prime}) \in \mathcal{E}_e} \left[W_e\left(E^{(e)} - E^{(e)\prime}\right) + W_e^*\left(S^{(e)} - S^{(e)\prime}\right) \right],$$

where

$$W_e(E^{(e)}) = \frac{1}{2} C_e E^{(e)2}, \quad W_e^*(S^{(e)}) = \frac{1}{2} \frac{S^{(e)2}}{C_e}.$$

Then the global penalty function measures the distance between the global state consisting of the assemblage of local states for individual bars and the given global data set. It can be defined as

$$F(\mathbf{E}, \mathbf{S}) = \sum_{e=1}^{N_e} w_e F_e(E^{(e)}, S^{(e)}).$$

The boldface notation in this formula collects the strain and stress states stored in all truss elements, namely

$$\mathbf{E} = \{E^{(e)}\}_{e=1}^{N_e}, \quad \mathbf{S} = \{S^{(e)}\}_{e=1}^{N_e}.$$

Recalling the derivation in the last section, it is reasonable to choose w_e to be the volume of the e-th truss member in the undeformed configuration. Although this choice naturally comes from the general penalty function (3), it should be highlighted here that the choice of these weight factors is not unique. The solver searches through all the possible data in a finite collection of values in the phase space for the best candidate with respect to some measure. Such best solution could be able to minimize a different distance measure that consists of a different use of positive weight factors. In mathematical terms, provided that the parameters C_e are fixed, we may say that those different choices of weight factors from which the same optimal solution can be attained lead to equivalent metrics on the phase space. Then one can also question why the volumes of elements are chosen. The answer is that we desire to maintain the consistency with the principle of virtual work so that the eventual formulation can be simplified. Plus, by using the volume weights, the intrinsically numerical parameters C_e appear to be consistent with the tangent constitutive matrix in terms of physical units. Apparently one may also argue that w_e can be absorbed in the parameters C_e and thus w_e are no longer necessary.

In the second step, we incorporate the strain definition and the principle of virtual work into the data-driven model. For a typical truss element the Green–Lagrange strain is given by

$$E^{(e)} = \mathbf{B}_0^{(e)} \mathbf{u}^{(e)} + \frac{1}{2} \mathbf{u}^{(e)\top} \mathbf{H} \mathbf{u}^{(e)}, \quad \mathbf{u} = [\, u \quad v \quad w \,]^\top. \tag{20}$$

The operators $\mathbf{B}_0^{(e)}$ and $\mathbf{H}$ acting on the element displacements are given by

$$\mathbf{B}_0^{(e)} = \frac{1}{L_0^{(e)}} \begin{bmatrix} -c_{0X}^{(e)} & -c_{0Y}^{(e)} & -c_{0Z}^{(e)} & c_{0X}^{(e)} & c_{0Y}^{(e)} & c_{0Z}^{(e)} \end{bmatrix},$$

$$\mathbf{H} = \frac{1}{L_0^{(e)2}} \begin{bmatrix} \mathbf{I}_3 & \mathbf{0} \\ \mathbf{0} & \mathbf{I}_3 \end{bmatrix}, \quad \mathbf{I}_3 = \begin{bmatrix} 1 & 0 & 0 \\ 0 & 1 & 0 \\ 0 & 0 & 1 \end{bmatrix},$$

where $c_{0\alpha}^{(e)}$, $\alpha = X, Y, Z$, are the direction cosines of the truss element axis in the undeformed configuration measured in the global Cartesian coordinates.

As we associate each truss member with only one local strain-stress state, the element internal force corresponding to the resultant stress can be derived from the principle of virtual work with relative ease and given as follows

$$\mathbf{P}^{(e)} = V_0^{(e)} S^{(e)} \mathbf{B}^{(e)}(\mathbf{u}^{(e)}), \tag{21}$$

where $V_0^{(e)} = A_0^{(e)} L_0^{(e)}$ is the volume of the truss element in the undeformed configuration, and

[3] We use the superscript to indicate the element-wise computation level instead of the subscript as it turns out more convenient for subsequent calculation and implementation. The element tangent stiffness is directly revealed.

$$\mathbf{B}^{(e)}(\mathbf{d}^{(e)}) = \mathbf{B}_0^{(e)} + \mathbf{d}^{(e)\top}\mathbf{H} = \mathbf{B}_0^{(e)} + \mathbf{B}_1^{(e)}(\mathbf{d}^{(e)}). \tag{22}$$

For the derivation of this result we refer the reader to the textbooks by Bathe [25] and Wriggers [42],[4] yet a computation of the internal force for the two-dimensional continuum body is illustrated in the next section. The structure internal force is obtained through the assemblage of element internal forces

$$\mathbf{P} = \mathop{\mathsf{A}}_{e=1}^{N_e} V_0^{(e)} S^{(e)} \mathbf{B}^{(e)}(\mathbf{u}^{(e)}).$$

We are eventually ready to write down the effective objective function

$$\begin{aligned}\Pi = &\sum_{e=1}^{N_e} w_e \left[W_e(E^{(e)} - E^{(e)*}) + W_e^*(S^{(e)} - S^{(e)*}) \right] \\ &- \sum_{i=1}^{N} \eta_i \left[\sum_{e=1}^{N} V_0^{(e)} S_e B_{ei}(\mathbf{u}) - f_i \right],\end{aligned} \tag{23}$$

where the matrix $\mathbf{B}$ without the superscript collects appropriately the element-wise matrices $\mathbf{B}^{(e)}$ in accordance with the finite element assemblage (compare [25,43]) and $\mathbf{f} = \{f_i\}_{i=1}^N$ is the nodal external force vector. The introduction of this matrix helps to write Π in a compact fashion. The pattern of mapping back to the element tangent stiffness is easily recognized. Analogously, the matrix $\mathbf{B}_0$ collects the components of $\mathbf{B}_0^{(e)}$ using the same mapping as for $\mathbf{B}$. In this manner, we may write

$$B_{ei} = [B_0]_{ei} + \sum_{j=1}^{N} H_{ji}^{(e)} u_j, \quad E^{(e)} = \sum_{i=1}^{N} [B_0]_{ei} u_i + \frac{1}{2} \sum_{i=1}^{N} \sum_{j=1}^{N} H_{ij}^{(e)} u_i u_j.$$

Substituting these expressions into (23), it can be explicitly written as

$$\begin{aligned}\Pi = &\sum_{e=1}^{N_e} w_e \left[W_e \left(\sum_{i=1}^{N} [B_0]_{ei} u_i + \frac{1}{2} \sum_{i=1}^{N} \sum_{j=1}^{N} H_{ij}^{(e)} u_i u_j - E^{(e)*} \right) + W_e^*(S^{(e)} - S^{(e)*}) \right] \\ &- \sum_{i=1}^{N} \eta_i \left[\sum_{e=1}^{N_e} V_0^{(e)} S^{(e)} \left([B_0]_{ei} + \sum_{j=1}^{N} H_{ij}^{(e)} u_j \right) - f_i \right].\end{aligned}$$

The first variation of Π is computed as follows

$$\begin{aligned}\delta\Pi = &\sum_{i=1}^{N} \left\{ \sum_{e=1}^{N_e} w_e C_e \left(\sum_{j=1}^{N} [B_0]_{ej} u_j + \frac{1}{2} \sum_{k=1}^{N} \sum_{l=1}^{N} H_{kl}^{(e)} u_k u_l - E^{(e)*} \right) B_{ei}(\mathbf{u}) \right. \\ &\left. - \sum_{e=1}^{N_e} V_0^{(e)} S^{(e)} \sum_{j=1}^{N} H_{ji}^{(e)} \eta_j \right\} \delta u_i + \sum_{e=1}^{N_e} \left\{ w_e \frac{1}{C_e} \left[S^{(e)} - S^{(e)*} \right] \right. \\ &\left. - \sum_{i=1}^{N} V_0^{(e)} B_{ei}(\mathbf{u}) \eta_i \right\} \delta S^{(e)} - \sum_{i=1}^{N} \left\{ \sum_{e=1}^{N_e} V_0^{(e)} S^{(e)} B_{ei}(\mathbf{u}) - f_i \right\} \delta\eta_i.\end{aligned}$$

Thus, invoking the stationarity of Π, we obtain the system of equations

$$\begin{aligned}&\sum_{e=1}^{N_e} w_e C_e \left(\sum_{j=1}^{N} [B_0]_{ej} u_j + \frac{1}{2} \sum_{i=1}^{N} \sum_{j=1}^{N} H_{ij}^{(e)} u_i u_j - E^{(e)*} \right) B_{ei}(\mathbf{u}) \\ &\qquad - \sum_{e=1}^{N_e} V_0^{(e)} S^{(e)} \sum_{j=1}^{N} H_{ji}^{(e)} \eta_j = 0, \quad i = 1, \dots, N, \\ &w_e \frac{1}{C_e} \left[S^{(e)} - S^{(e)*} \right] - \sum_{i=1}^{N} V_0^{(e)} B_{ei}(\mathbf{u}) \eta_i = 0, \quad e = 1, \dots, N_e, \\ &\sum_{e=1}^{N_e} V_0^{(e)} S_e B_{ei}(\mathbf{u}) - f_i = 0, \quad i = 1, \dots, N.\end{aligned} \tag{24}$$

[4] Extra computation is needed.

The second equation can be resolved for $S^{(e)}$ to obtain

$$S^{(e)} = V_0^{(e)} \frac{w_e}{C_e} \sum_{i=1}^{N} B_{ei}(\mathbf{u}) \eta_i + S^{(e)*}. \tag{25}$$

Again, it is seen that if the element stress only pertains to its element, the stress can be statically condensed from the system leaving the equations depending only on displacements and Lagrange multipliers. Plugging the identity (25) into Eqs. $(24)_1$ and $(25)_3$, we end up with two lengthy equations. Despite the explicit form of these nonlinear algebraic equations, the expression prevents insight into the implementation process.

We know that in an actual implementation within the context of the finite element method the summation over all elements are conducted by the assembly process. The aim of the preceding calculation is to realize that the structural Eqs. (24) can be engendered to

$$\begin{aligned}&\mathop{\mathsf{A}}_{e=1}^{N_e} \left\{ w_e C_e \left[E^{(e)}(\mathbf{u}^{(e)}) - E^{(e)*} \right] \mathbf{B}^{(e)\top}(\mathbf{u}^{(e)}) - V_0^{(e)} S^{(e)} \mathbf{H} \boldsymbol{\eta}^{(e)} \right\} = \mathbf{0}, \\ &\frac{w_e}{C_e} \left[S^{(e)} - S^{(e)*} \right] - V_0^{(e)} \mathbf{B}^{(e)}(\mathbf{u}^{(e)}) \boldsymbol{\eta}^{(e)} = 0, \\ &\mathop{\mathsf{A}}_{e=1}^{N_e} \left\{ V_0^{(e)} S^{(e)} \mathbf{B}^{(e)\top}(\mathbf{u}^{(e)}) \right\} = \mathbf{f},\end{aligned}$$

where the element degrees of freedom $\boldsymbol{\eta}^{(e)}$ are obtained from the structure counterpart by the same mapping as for the displacement $\mathbf{u}^{(e)}$. Eliminating $S^{(e)}$ from the second equation, we obtain

$$\begin{aligned}&\mathop{\mathsf{A}}_{e=1}^{N_e} \left\{ w_e C_e \left[E^{(e)}(\mathbf{u}^{(e)}) - E^{(e)*} \right] \mathbf{B}^{(e)\top}(\mathbf{u}^{(e)}) - V_0^{(e)} S(\mathbf{u}^{(e)}, \boldsymbol{\eta}^{(e)}) \mathbf{H} \boldsymbol{\eta}^{(e)} \right\} = \mathbf{0}, \\ &\mathop{\mathsf{A}}_{e=1}^{N_e} \left\{ V_0^{(e)} S(\mathbf{u}^{(e)}, \boldsymbol{\eta}^{(e)}) \mathbf{B}^{(e)\top}(\mathbf{u}^{(e)}) \right\} = \mathbf{f},\end{aligned} \tag{26}$$

in which we have written the system in form of column vectors and

$$S(\mathbf{u}^{(e)}, \boldsymbol{\eta}^{(e)}) = \frac{C_e}{w_e} V_0^{(e)} \mathbf{B}^{(e)}(\mathbf{u}^{(e)}) \boldsymbol{\eta}^{(e)} + S^{(e)*}.$$

On the element level, it suffices to consider the two element generalized internal force vectors

$$\begin{aligned}\mathbf{P}_{\mathbf{u}}^{(e)} &= w_e C_e \left[E^{(e)}(\mathbf{u}^{(e)}) \mathbf{B}^{(e)\top}(\mathbf{u}^{(e)}) - E^{(e)*} \mathbf{B}_1^{(e)\top}(\mathbf{u}^{(e)}) \right] \\ &\quad - V_0^{(e)} S(\mathbf{u}^{(e)}, \boldsymbol{\eta}^{(e)}) \mathbf{H} \boldsymbol{\eta}^{(e)}, \\ \mathbf{P}_{\boldsymbol{\eta}}^{(e)} &= V_0^{(e)} S(\mathbf{u}^{(e)}, \boldsymbol{\eta}^{(e)}) \mathbf{B}^{(e)\top}(\mathbf{u}^{(e)}),\end{aligned}$$

and the element generalized external force vector

$$\mathbf{F}_{E^*}^{(e)} = w_e C_e E^{(e)*} \mathbf{B}_0^{(e)\top}. \tag{27}$$

System (26) is solved by using the Newton-Raphson method. To this end, we need to compute the element tangent stiffness matrix

$$\mathbf{K}^{(e)} = \begin{bmatrix} \dfrac{\partial \mathbf{P}_{\mathbf{u}}^{(e)}}{\partial \mathbf{u}^{(e)}} & \dfrac{\partial \mathbf{P}_{\mathbf{u}}^{(e)}}{\partial \boldsymbol{\eta}^{(e)}} \\ \dfrac{\partial \mathbf{P}_{\boldsymbol{\eta}}^{(e)}}{\partial \mathbf{u}^{(e)}} & \dfrac{\partial \mathbf{P}_{\boldsymbol{\eta}}^{(e)}}{\partial \boldsymbol{\eta}^{(e)}} \end{bmatrix}.$$

After some algebraic manipulation, we arrive at

$$\begin{aligned}
\frac{\partial \mathbf{P}_{\mathbf{u}}^{(e)}}{\partial \mathbf{u}^{(e)}} &= w_e C_e \Big\{ \mathbf{B}^{(e)\top}(\mathbf{u}^{(e)}) \mathbf{B}^{(e)}(\mathbf{u}^{(e)}) + \Big[E^{(e)}(\mathbf{u}^{(e)}) - E^{(e)*} \Big] \mathbf{H} \Big\} \\
&\quad - V_0^{(e)2} \frac{C_e}{w_e} \mathbf{B}_1^{(e)\top}(\boldsymbol{\eta}^{(e)}) \mathbf{B}_1^{(e)}(\boldsymbol{\eta}^{(e)}), \\
\frac{\partial \mathbf{P}_{\mathbf{u}}^{(e)}}{\partial \boldsymbol{\eta}^{(e)}} &= -V_0^{(e)} \Big[V_0^{(e)} \frac{C_e}{w_e} \mathbf{B}_1^{(e)\top}(\boldsymbol{\eta}^{(e)}) \mathbf{B}^{(e)}(\mathbf{u}^{(e)}) + S(\mathbf{u}^{(e)}, \boldsymbol{\eta}^{(e)}) \mathbf{H} \Big], \\
\frac{\partial \mathbf{P}_{\boldsymbol{\eta}}^{(e)}}{\partial \mathbf{u}^{(e)}} &= V_0^{(e)} \Big[V_0^{(e)} \frac{C_e}{w_e} \mathbf{B}^{(e)\top}(\mathbf{u}^{(e)}) \mathbf{B}_1^{(e)}(\boldsymbol{\eta}^{(e)}) + S(\mathbf{u}^{(e)}, \boldsymbol{\eta}^{(e)}) \mathbf{H} \Big], \\
\frac{\partial \mathbf{P}_{\boldsymbol{\eta}}^{(e)}}{\partial \boldsymbol{\eta}^{(e)}} &= V_0^{(e)2} \frac{C_e}{w_e} \mathbf{B}^{(e)\top}(\mathbf{u}^{(e)}) \mathbf{B}^{(e)}(\mathbf{u}^{(e)}),
\end{aligned} \tag{28}$$

where

$$\mathbf{B}^{(e)} = \mathbf{B}_0^{(e)} + \mathbf{u}^{(e)\top} \mathbf{H}, \quad \mathbf{B}_1^{(e)} = \boldsymbol{\eta}^{(e)\top} \mathbf{H}.$$

We have kept w_e general in this formula. By virtue of the argument at the beginning of this section, setting $w_e = V_0^{(e)}$ in the above expressions gives

$$\begin{aligned}
\frac{\partial \mathbf{P}_{\mathbf{u}}^{(e)}}{\partial \mathbf{u}^{(e)}} &= V_0^{(e)} C_e \Big\{ \mathbf{B}^{(e)\top} \mathbf{B}^{(e)} + \Big[E^{(e)} - E^{(e)*} \Big] \mathbf{H} - \mathbf{B}_1^{(e)\top} \mathbf{B}_1^{(e)} \Big\}, \\
\frac{\partial \mathbf{P}_{\mathbf{u}}^{(e)}}{\partial \boldsymbol{\eta}^{(e)}} &= -V_0^{(e)} \Big\{ C_e \mathbf{B}_1^{(e)\top} \mathbf{B}^{(e)} + S(\mathbf{u}^{(e)}, \boldsymbol{\eta}^{(e)}) \mathbf{H} \Big\}, \\
\frac{\partial \mathbf{P}_{\boldsymbol{\eta}}^{(e)}}{\partial \mathbf{u}^{(e)}} &= +V_0^{(e)} \Big\{ C_e \mathbf{B}^{(e)\top} \mathbf{B}_1^{(e)} + S(\mathbf{u}^{(e)}, \boldsymbol{\eta}^{(e)}) \mathbf{H} \Big\}, \\
\frac{\partial \mathbf{P}_{\boldsymbol{\eta}}^{(e)}}{\partial \boldsymbol{\eta}^{(e)}} &= V_0^{(e)} C_e \mathbf{B}^{(e)\top} \mathbf{B}^{(e)}.
\end{aligned} \tag{29}$$

The simplification of (28) to (29) heuristically justifies why we have chosen $w_e = V_0^{(e)}$. Note that the tangent stiffness is anti-symmetric. Of course it will be symmetric if we change the sign of $\mathbf{P}_{\boldsymbol{\eta}}$. The solution is achieved by following the iteration formula (15) with the tangent stiffness matrix and the generalized external force vectors being computed from (27) and (29), respectively, and then assembled.

This result reduces to that for the linear elasticity data-driven solver when the linearized strain is used. Indeed, in this case we simply identify $\mathbf{H} = \mathbf{0}$, and thus $\mathbf{B}^{(e)} = \mathbf{B}_0^{(e)}$, $\mathbf{B}_1^{(e)} = \mathbf{0}$, to obtain the stiffness matrix in [16].

Note that our definition of the cost function (3) is rather straight-forward and might be the simplest (however, not at all optimal) one. In fact, in the given simple case where the second Piola-Kirchhoff stress depends linearly on the Green-Lagrange strain (in the form of a Saint-Venant-Kirchhoff material law) poly-convexity is lost, see e.g. Ibrahimbegovic [22]. Thus, better choices of cost functions will lead to strong improvements of data mining in nonlinear elasticity. One such choice could be the adjustment of the cost function to the form of a neo-Hookean material law. However, such adjustments are beyond the scope of the current contribution. Instead, we refrain from touching the point where instabilities, neither structural nor material instabilities, may happen.

In the same affair, it must be aware that as the data-driven solver relies itself solely on the experimental data, the collected data could be corrupted by instability phenomena. To break it down, let us imagine that the material data is collected by a set of uniaxial compression-tension tests on one single bar. The compression-tension test data could be obtained until instabilities may occur. However, when a more complicated geometry of the system is constituted so that instabilities such as snap-through and bucking phenomena may happen in a range in which the data have not been available, then we lack the data, or even the most nearest, to detect such instabilities. We again would like to emphasize that in this work we do not consider stability phenomena and assume that the given data is not corrupted by such issues. To be specific, in order to avoid stability issues in our numerical simulations, we constantly check the overall stiffness including the artificial stiffness introduced by the penalty function and only conduct the simulations when classical instabilities do not happen.

3.2. Numerical example

We study a structure of 39 truss elements visualized in Fig. 8. The prescribed degrees of freedom and the externally applied loads are also depicted. As explained above, the solution of such idealized truss model is exactly the finite element solution since distributed forces along the truss elements are not considered. For this reason, by comparing the data-driven solution with the reference finite element solution, we are actually performing a comparison with the exact one. The reference solution is achieved by using the finite element incremental procedure (cf. [25]). In this example we examine the convergence of the solution with respect to the data size. To be precise, the experiment is conducted on a sequence of data sets that are obtained in the following manner. First, a set of data is coarsely generated from the Mooney-Rivlin model (19), then the next set is obtained by halving the distance between two strain values and placing an extra value in between. That is, the next set has as doubly many material data points as the last set. In Fig. 9 the error norms between the data-driven strain

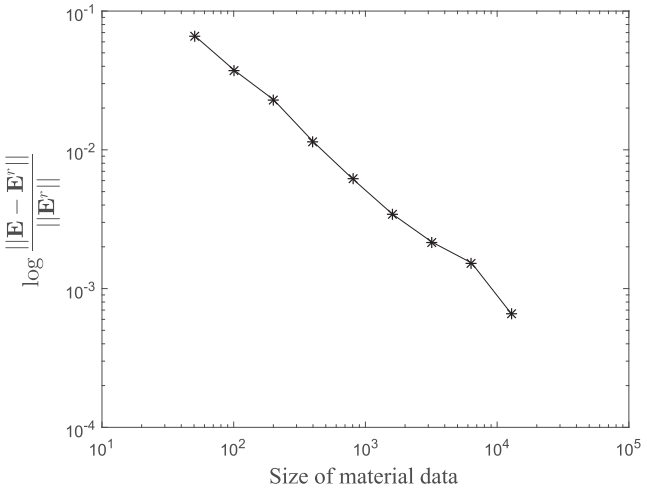

Fig. 9. Convergence of data-driven strain solution with respect to the data size.

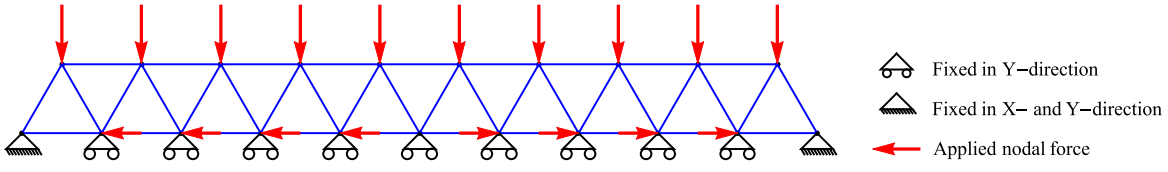

Fig. 8. A simple truss structure with essential boundary conditions and externally applied loads.

solution and the reference strain solution are plotted for data sets with increasing size. We observe that the data-driven strain solution converges to the reference one as the data size is uniformly enriched. Furthermore, the convergence rate of about a half is realizable.

4. Data-driven solver for nonlinear plane stress problems

Moving forward with a two-dimensional problem, we consider a plane stress problem within the finite strain theory. In this case the phase space consists of pairs of the Green-Lagrange strain and the second Piola-Kirchhoff stress tensors appeared as $(\mathbf{E},\mathbf{S})$. Since we restrict ourselves to the plane stress case, the corresponding phase space is six-dimensional taking into account the symmetry property of strain and stress.

4.1. Mathematical formulation

In the first attempt of dealing with the nonlinear problem let us start with a simple formulation by studying the data-driven problem with the help of linear triangular elements. It suffices to associate with each element one single strain-stress pair, denoted by $(\mathbf{E}^{(e)},\mathbf{S}^{(e)})$, $e=1,\dots,N_e$.

The flowchart is similar to that of the last sections. We start with the local penalty function for each element

$$\begin{aligned} F_e(\mathbf{E}^{(e)},\mathbf{S}^{(e)}) &= \min_{(\mathbf{E}^{(e)\prime},\mathbf{S}^{(e)\prime})\in\mathcal{E}_e}\Big[W_e(\mathbf{E}^{(e)}-\mathbf{E}^{(e)\prime})+W_e^*(\mathbf{S}^{(e)}-\mathbf{S}^{(e)\prime})\Big],\\ W_e(\mathbf{E}^{(e)}) &= \frac{1}{2}\mathbf{E}^{(e)}\cdot\mathbf{C}_e\mathbf{E}^{(e)},\quad W_e^*(\mathbf{S}^{(e)}) = \frac{1}{2}\mathbf{S}^{(e)}\cdot\mathbf{C}_e^{-1}\mathbf{S}^{(e)}, \end{aligned} \tag{30}$$

where the strain and the stress are written in the Voigt representation

$$\mathbf{E}^{(e)} = \begin{bmatrix} E_{11}^{(e)} & E_{22}^{(e)} & 2E_{12}^{(e)}\end{bmatrix}^\top,\quad \mathbf{S}^{(e)} = \begin{bmatrix} S_{11}^{(e)} & S_{22}^{(e)} & S_{12}^{(e)}\end{bmatrix}^\top,$$

and $\mathbf{C}_e$ is the matrix-valued parameter associated with each element. It suffices to choose symmetric matrices as only the symmetric parts of $\mathbf{C}_e$ involve in the first variation.

Next, we need to cast the principle of virtual work to the equation of equilibrium between the internal force and external force (see for example (21)). It is instructive to illustrate how we can obtain the internal force from the internal energy stored in the body by imposing the virtual displacement field on the body. Let us examine the virtual internal work within one triangular element

$$I^{(e)} = \int_{V_0^{(e)}} S_{ij}^{(e)}\delta E_{ij}^{(e)}\mathrm{d}V = \int_{V_0^{(e)}}\Big[S_{11}^{(e)}\delta E_{11}^{(e)}+S_{22}^{(e)}\delta E_{22}^{(e)}+2S_{12}^{(e)}\delta E_{12}^{(e)}\Big]\mathrm{d}V.$$

There is no need to write the superscript (e) on the strain field as the integral on the element volume $V_0^{(e)}$ indicates that only the strain energy within the e-th element is computed. But the superscript on the stress values is needed since it indicates the values associated with the corresponding element. As we use the linear triangular element, the virtual strain is constant throughout each element. We shall suppress the superscript (e) on the strain and stress in the derivation of the internal force. Then we may write

$$I^{(e)} = V_0^{(e)}[S_{11}\delta E_{11}+S_{22}\delta E_{22}+2S_{12}\delta E_{12}]. \tag{31}$$

We compute the Green-Lagrange strain in terms of the displacement degrees of freedom. Using the linear triangular element, the displacements can be interpolated as follows

$$u(x,y) = \mathbf{\Phi}(X,Y)\mathbf{u},\quad v(X,Y) = \mathbf{\Phi}(X,Y)\mathbf{v},$$

where

$$\mathbf{\Phi}(X,Y) = [\,\phi_1\ \phi_2\ \phi_3\,],\quad \mathbf{u} = \begin{bmatrix} u_1^{(e)} & u_2^{(e)} & u_3^{(e)}\end{bmatrix}^\top,\quad \mathbf{v} = \begin{bmatrix} v_1^{(e)} & v_2^{(e)} & v_3^{(e)}\end{bmatrix}^\top.$$

By definition, we have

$$E_{11} = \mathbf{\Phi}_X\mathbf{u}+\frac{1}{2}(\mathbf{\Phi}_X\mathbf{u})^2+\frac{1}{2}(\mathbf{\Phi}_X\mathbf{v})^2,$$

$$E_{22} = \mathbf{\Phi}_Y\mathbf{v}+\frac{1}{2}(\mathbf{\Phi}_Y\mathbf{u})^2+\frac{1}{2}(\mathbf{\Phi}_Y\mathbf{v})^2,$$

$$2E_{12} = \mathbf{\Phi}_Y\mathbf{u}+\mathbf{\Phi}_X\mathbf{v}+(\mathbf{\Phi}_X\mathbf{u})(\mathbf{\Phi}_Y\mathbf{u})+(\mathbf{\Phi}_X\mathbf{v})(\mathbf{\Phi}_Y\mathbf{v}).$$

We collect $\mathbf{u}$ and $\mathbf{v}$ into the column vector $\mathbf{q}$ in the following order

$$\mathbf{q} = [\,u_1\quad v_1\quad u_2\quad v_2\quad u_3\quad v_3\,]^\top,$$

and rewrite the above expressions as

$$\begin{aligned} E_{11} &= \mathbf{Q}_1\mathbf{q}+\frac{1}{2}\mathbf{q}^\top(\mathbf{A}_1+\mathbf{A}_2)\mathbf{q},\\ E_{22} &= \mathbf{Q}_2\mathbf{q}+\frac{1}{2}\mathbf{q}^\top(\mathbf{A}_3+\mathbf{A}_4)\mathbf{q},\\ 2E_{12} &= \mathbf{Q}_3\mathbf{q}+\mathbf{q}^\top(\mathbf{A}_5+\mathbf{A}_6)\mathbf{q}, \end{aligned} \tag{32}$$

where the matrices $\mathbf{Q}_j$, $j=1,2,3$, and $\mathbf{A}_j$, $j=1,\dots,6$, are given by

$$\mathbf{Q}_1 = [\,\phi_{1,X}\quad 0\quad \phi_{2,X}\quad 0\quad \phi_{3,X}\quad 0\,],$$

$$\mathbf{Q}_2 = [\,0\quad \phi_{1,Y}\quad 0\quad \phi_{2,Y}\quad 0\quad \phi_{3,Y}\,],$$

$$\mathbf{Q}_3 = [\,\phi_{1,Y}\quad \phi_{1,X}\quad \phi_{2,Y}\quad \phi_{2,X}\quad \phi_{3,Y}\quad \phi_{3,X}\,],$$

and

$$\mathbf{A}_1 = [\,\phi_{1,X}\quad 0\quad \phi_{2,X}\quad 0\quad \phi_{3,X}\quad 0\,]^\top[\,\phi_{1,X}\quad 0\quad \phi_{2,X}\quad 0\quad \phi_{3,X}\quad 0\,],$$

$$\mathbf{A}_2 = [\,0\quad \phi_{1,X}\quad 0\quad \phi_{2,X}\quad 0\quad \phi_{3,X}\,]^\top[\,0\quad \phi_{1,X}\quad 0\quad \phi_{2,X}\quad 0\quad \phi_{3,X}\,],$$

$$\mathbf{A}_3 = [\,\phi_{1,Y}\quad 0\quad \phi_{2,Y}\quad 0\quad \phi_{3,Y}\quad 0\,]^\top[\,\phi_{1,Y}\quad 0\quad \phi_{2,Y}\quad 0\quad \phi_{3,Y}\quad 0\,],$$

$$\mathbf{A}_4 = [\,0\quad \phi_{1,Y}\quad 0\quad \phi_{2,Y}\quad 0\quad \phi_{3,Y}\,]^\top[\,0\quad \phi_{1,Y}\quad 0\quad \phi_{2,Y}\quad 0\quad \phi_{3,Y}\,],$$

$$\mathbf{A}_5 = [\,\phi_{1,X}\quad 0\quad \phi_{2,X}\quad 0\quad \phi_{3,X}\quad 0\,]^\top[\,\phi_{1,Y}\quad 0\quad \phi_{2,Y}\quad 0\quad \phi_{3,Y}\quad 0\,],$$

$$\mathbf{A}_6 = [\,0\quad \phi_{1,X}\quad 0\quad \phi_{2,X}\quad 0\quad \phi_{3,X}\,]^\top[\,0\quad \phi_{1,Y}\quad 0\quad \phi_{2,Y}\quad 0\quad \phi_{3,Y}\,].$$

By denoting

$$\mathbf{H}_1 = \mathbf{A}_1+\mathbf{A}_2,\quad \mathbf{H}_2 = \mathbf{A}_3+\mathbf{A}_4,\quad \mathbf{H}_3 = (\mathbf{A}_5+\mathbf{A}_6)+(\mathbf{A}_5+\mathbf{A}_6)^\top,$$

the strain components can be written in the following compact form

$$\begin{aligned} E_{11} &= \mathbf{Q}_1\mathbf{q}+\frac{1}{2}\mathbf{q}^\top\mathbf{H}_1\mathbf{q},\\ E_{22} &= \mathbf{Q}_2\mathbf{q}+\frac{1}{2}\mathbf{q}^\top\mathbf{H}_2\mathbf{q},\\ 2E_{12} &= \mathbf{Q}_3\mathbf{q}+\frac{1}{2}\mathbf{q}^\top\mathbf{H}_3\mathbf{q}. \end{aligned} \tag{33}$$

Now it is straightforward to compute the variation in strain

$$\begin{aligned} \delta E_{11} &= \delta\mathbf{q}^\top(\mathbf{Q}_1^\top+\mathbf{H}_1\mathbf{q}),\\ \delta E_{22} &= \delta\mathbf{q}^\top(\mathbf{Q}_2^\top+\mathbf{H}_2\mathbf{q}),\\ 2\delta E_{12} &= \delta\mathbf{q}^\top(\mathbf{Q}_3^\top+\mathbf{H}_3\mathbf{q}). \end{aligned}$$

Substituting these variations into the internal virtual work (30), we arrive at

$$I^{(e)} = \delta\mathbf{q}^\top\Big\{V_0^{(e)}[S_{11}(\mathbf{Q}_1^\top+\mathbf{H}_1\mathbf{q})+S_{22}(\mathbf{Q}_2^\top+\mathbf{H}_2\mathbf{q})+S_{12}(\mathbf{Q}_3^\top+\mathbf{H}_3\mathbf{q})]\Big\}$$

If we multiply out $\mathbf{H}_i\mathbf{q}$ and then plug the matrices $\mathbf{Q}_i^\top + \mathbf{H}_i\mathbf{q}$ into one common matrix

$$\mathbf{B}(\mathbf{q}) = \begin{bmatrix} \mathbf{Q}_1 + \mathbf{q}^\top\mathbf{H}_1 \\ \mathbf{Q}_2 + \mathbf{q}^\top\mathbf{H}_2 \\ \mathbf{Q}_3 + \mathbf{q}^\top\mathbf{H}_3 \end{bmatrix},$$

we recognize that $\mathbf{B}$ is identical to the linear part of B-matrix, namely ${}^t_0\mathbf{B}_L$, given in [25]. This is not surprising by all means: The matrix $\mathbf{B}$ in our computation is derived from the formula that resembles the linear part of the internal virtual work in the incremental procedure after linearization. For convenience of further computation, we decompose $\mathbf{B}(\mathbf{q})$ into two matrices $\mathbf{B}_0$ and $\mathbf{B}_1(\mathbf{q})$ defined by

$$\mathbf{B}_0 = \begin{bmatrix} \mathbf{Q}_1 \\ \mathbf{Q}_2 \\ \mathbf{Q}_3 \end{bmatrix}, \quad \mathbf{B}_1(\mathbf{d}) = \begin{bmatrix} \mathbf{d}^\top\mathbf{H}_1 \\ \mathbf{d}^\top\mathbf{H}_2 \\ \mathbf{d}^\top\mathbf{H}_3 \end{bmatrix}.$$

Note that this practice has been repeatedly done in the last sections. Restoring the indication (e) over the element matrices, we eventually arrive at the element nodal internal force as the column vector

$$\begin{aligned}\mathbf{P}^{(e)} = V_0^{(e)}\Big\{ & S_{11}^{(e)}\Big[\mathbf{Q}_1^{(e)\top} + \mathbf{H}_1^{(e)}\mathbf{q}^{(e)}\Big] + S_{22}^{(e)}\Big[\mathbf{Q}_2^{(e)^\top} + \mathbf{H}_2^{(e)}\mathbf{q}^{(e)}\Big] \\ & + S_{12}^{(e)}\Big[\mathbf{Q}_3^{(e)\top} + \mathbf{H}_3^{(e)}\mathbf{q}^{(e)}\Big]\Big\}. \end{aligned} \tag{34}$$

Having three ingredients (30), (33), (34), we can write down the effective objective function

$$\Pi = \sum_{e=1}^{N_e} w_e F_e\Big(\mathbf{E}^{(e)}, \mathbf{S}^{(e)}\Big) - \sum_{j=1}^{N}\eta_j[P_j - f_j],$$

where $\mathbf{f} = (f_i)$ is the external force vector computed by using the same mesh of linear triangular elements. We choose the weight factors $w_e = V_0^{(e)} = tA_0^{(e)}$, where t is the thickness of the body under consideration, $A_0^{(e)}$ is area of the e-th element in the undeformed configuration. Instead of expanding the objective function in terms of the nodal displacements and invoking the global variation $\delta\Pi = 0$, we shall manipulate the computation of the element objective function

$$\begin{aligned}\Pi^{(e)} = V_0^{(e)}\Big[& \frac{1}{2}(\mathbf{E}^{(e)} - \mathbf{E}^{(e)*})^\top\mathbf{C}_e(\mathbf{E}^{(e)} - \mathbf{E}^{(e)*}) + \frac{1}{2}(\mathbf{S}^{(e)} - \mathbf{S}^{(e)*})^\top\mathbf{C}_e^{-1}(\mathbf{S}^{(e)} - \mathbf{S}^{(e)*})\Big] \\ & - \boldsymbol{\eta}^{(e)\top}\Big[\mathbf{P}^{(e)}(\mathbf{q}^{(e)}) - \mathbf{f}^{(e)}\Big].\end{aligned}$$

The first variation of $\Pi^{(e)}$ is given by

$$\delta\Pi^{(e)} = \frac{\partial\Pi^{(e)}}{\partial\mathbf{q}^{(e)}}\cdot\delta\mathbf{q}^{(e)} + \frac{\partial\Pi^{(e)}}{\partial\mathbf{S}^{(e)}}\cdot\delta\mathbf{S}^{(e)} + \frac{\partial\Pi^{(e)}}{\partial\boldsymbol{\eta}^{(e)}}\cdot\delta\boldsymbol{\eta}^{(e)},$$

where the partial derivatives of $\Pi^{(e)}$ are computed as follows

$$\begin{aligned}\frac{\partial\Pi^{(e)}}{\partial\mathbf{q}^{(e)}} &= V_0^{(e)}\Big\{\mathbf{B}^\top(\mathbf{q}^{(e)})\mathbf{C}_e\Big[\mathbf{E}^{(e)}(\mathbf{q}^{(e)}) - \mathbf{E}^{(e)*}\Big] - \mathbf{B}_1^\top(\boldsymbol{\eta}^{(e)})\mathbf{S}^{(e)}\Big\}, \\ \frac{\partial\Pi^{(e)}}{\partial\mathbf{S}^{(e)}} &= V_0^{(e)}\Big\{\mathbf{C}_e^{-1}(\mathbf{S}^{(e)} - \mathbf{S}^{(e)*}) - \mathbf{B}(\mathbf{q}^{(e)})\boldsymbol{\eta}^{(e)}\Big\}, \\ \frac{\partial\Pi^{(e)}}{\partial\boldsymbol{\eta}^{(e)}} &= V_0^{(e)}\mathbf{B}^\top(\mathbf{q})\mathbf{S}^{(e)} - \mathbf{f}^{(e)}.\end{aligned} \tag{35}$$

From the equations corresponding to the variations $\delta S_{11}^{(e)}$, $\delta S_{22}^{(e)}$, $\delta S_{12}^{(e)}$, we find

$$\mathbf{S}^{(e)} = \mathbf{C}_e\mathbf{B}(\mathbf{q}^{(e)})\boldsymbol{\eta}^{(e)} + \mathbf{S}^{(e)*}. \tag{36}$$

We recall that this static condensation can only be carried out if the element stress pertains only to one element. Substituting it into the first and the last of (35), we obtain

$$\frac{\partial\Pi^{(e)}}{\partial\mathbf{q}^{(e)}} = V_0^{(e)}\Big\{\mathbf{B}^\top(\mathbf{q}^{(e)})\mathbf{C}_e\Big[\mathbf{E}^{(e)}(\mathbf{q}^{(e)}) - \mathbf{E}^{(e)*}\Big] - \mathbf{B}_1^\top(\boldsymbol{\eta}^{(e)})\Big[\mathbf{C}_e\mathbf{B}(\mathbf{q}^{(e)})\boldsymbol{\eta}^{(e)} + \mathbf{S}^{(e)*}\Big]\Big\},$$

$$\frac{\partial\Pi^{(e)}}{\partial\boldsymbol{\eta}^{(e)}} = V_0^{(e)}\mathbf{B}^{(e)\top}(\mathbf{q}^{(e)})\Big[\mathbf{C}_e\mathbf{B}(\mathbf{q}^{(e)})\boldsymbol{\eta}^{(e)} + \mathbf{S}^{(e)*}\Big] - \mathbf{f}^{(e)}.$$

Let us denote by $\mathbf{q}$ the system nodal displacements and order the degrees of freedom as follows

$$\mathbf{q} = [\,u_1 \quad v_1 \quad \dots \quad u_N \quad v_N\,]^\top,$$

and similarly by $\boldsymbol{\eta}$ the Lagrange multipliers corresponding to these nodal displacements

$$\boldsymbol{\eta} = [\,\eta_{1X} \quad \eta_{1Y} \quad \dots \quad \eta_{NX} \quad \eta_{NY}\,]^\top.$$

The contribution of all variations $\delta\Pi^{(e)}$ corresponds to the assemblage of the difference between the generalized internal force vector and the generalized external force vector multiplied by the variation in the generalized degrees of freedom consisting of the nodal displacements and the Lagrange multipliers at the respective nodes. This statement is expressed as

$$\begin{aligned}\delta\Pi = \sum_{e=1}^{N_e}\delta\Pi^{(e)} &= \sum_{e=1}^{N_e}\left[\frac{\partial\Pi^{(e)}}{\partial\mathbf{q}^{(e)}}\cdot\delta\mathbf{q}^{(e)} + \frac{\partial\Pi^{(e)}}{\partial\boldsymbol{\eta}^{(e)}}\cdot\delta\boldsymbol{\eta}^{(e)}\right] \\ &= \left[\mathop{\mathrm{A}}_{e=1}^{N_e}\frac{\partial\Pi^{(e)}}{\partial\mathbf{q}^{(e)}}\right]\cdot\delta\mathbf{q} + \left[\mathop{\mathrm{A}}_{e=1}^{N_e}\frac{\partial\Pi^{(e)}}{\partial\boldsymbol{\eta}^{(e)}}\right]\cdot\delta\boldsymbol{\eta}.\end{aligned}$$

Thus, the variational equation $\delta\Pi = 0$ leads to the system of algebraic equations

$$\mathop{\mathrm{A}}_{e=1}^{N_e}\mathbf{P}_{\mathbf{q}}^{(e)} = \mathbf{F}_{\mathbf{E}^*}, \quad \mathop{\mathrm{A}}_{e=1}^{N_e}\mathbf{P}_{\boldsymbol{\eta}}^{(e)} = \mathbf{f},$$

where

$$\begin{aligned}\mathbf{P}_{\mathbf{q}}^{(e)} &= V_0^{(e)}\Big\{\mathbf{B}^{(e)\top}(\mathbf{q}^{(e)})\mathbf{C}_e\mathbf{E}^{(e)}(\mathbf{q}^{(e)}) - \mathbf{B}_1(\mathbf{q}^{(e)})\mathbf{C}_e\mathbf{E}^{(e)*} \\ &\qquad -\mathbf{B}_1^\top(\boldsymbol{\eta}^{(e)})\Big[\mathbf{C}_e\mathbf{B}^{(e)}(\mathbf{q}^{(e)})\boldsymbol{\eta}^{(e)} + \mathbf{S}^{(e)*}\Big]\Big\}, \\ \mathbf{P}_{\boldsymbol{\eta}}^{(e)} &= V_0^{(e)}\mathbf{B}^{(e)\top}(\mathbf{q}^{(e)})\Big[\mathbf{C}_e\mathbf{B}^{(e)}(\mathbf{q}^{(e)})\boldsymbol{\eta}^{(e)} + \mathbf{S}^{(e)*}\Big], \\ \mathbf{F}_{\mathbf{E}^{(e)*}} &= V_0^{(e)}\mathbf{B}_0^{(e)\top}\mathbf{C}_e\mathbf{E}^{(e)*}.\end{aligned} \tag{37}$$

In order to apply the Newton-Raphson method, we compute the element tangent stiffness matrix

$$\mathbf{K}^{(e)} = \begin{bmatrix} \dfrac{\partial\mathbf{P}_{\mathbf{q}}^{(e)}}{\partial\mathbf{q}^{(e)}} & \dfrac{\partial\mathbf{P}_{\mathbf{q}}^{(e)}}{\partial\boldsymbol{\eta}^{(e)}} \\ \dfrac{\partial\mathbf{P}_{\boldsymbol{\eta}}^{(e)}}{\partial\mathbf{q}^{(e)}} & \dfrac{\partial\mathbf{P}_{\boldsymbol{\eta}}^{(e)}}{\partial\boldsymbol{\eta}^{(e)}} \end{bmatrix}. \tag{38}$$

The computation is carried on in the indicial notation. To this end, we rewrite $(37)_1$ and $(37)_2$ component-wisely as follows

$$\begin{aligned}[P_q]_i = V_0\Big\{ & C_{mk}\epsilon_k\big([B_0]_{mi} + [B_1(\mathbf{q})]_{mi}\big) - C_{mk}\epsilon_k^*[B_1(\mathbf{q})]_{mi} \\ & - \Big[C_{mn}\big([B_0]_{nk} + [B_1(\mathbf{q})]_{nk}\big)\eta_k + S_m^{(e)*}\Big][B_1(\boldsymbol{\eta})]_{mi}\Big\}, \\ [P_\eta]_i = V_0\big[C_{mn}\big([B_0]_{nk} + [B_1(\mathbf{q})]_{nk}\big)\eta_k + S_m^*\big]\big([B_0]_{mi} + [B_1(\mathbf{q})]_{mi}\big),\end{aligned}$$

where the superscript indication (e) is suppressed at this step and the Einstein summation is employed. In addition, the new denotation ϵ_k is used in replacement of the components of the strain $\mathbf{E}$ as follows

$$\epsilon_1 = E_{11}, \quad \epsilon_2 = E_{22}, \quad \epsilon_3 = 2E_{12}.$$

Then we have

$$\begin{aligned}
\frac{\partial [P_q]_i}{\partial q_j} &= V_0 \Big\{ C_{mk} \big([B_0]_{mi} + [B_1(\mathbf{q})]_{mi} \big) \Big([B_0]_{kj} + [B_1(\mathbf{q})]_{kj} \Big) + C_{mk} (\epsilon_k - \epsilon_k^*) \frac{\partial [B_1(\mathbf{q})]_{mi}}{\partial q_j} - C_{mn} \frac{\partial [B_1(\mathbf{q})]_{nk}}{\partial q_j} \eta_k [B_1(\boldsymbol{\eta})]_{mi} \Big\}, \\
\frac{\partial [P_\eta]_i}{\partial \eta_j} &= -V_0 \Big\{ C_{mn} [B_1(\boldsymbol{\eta})]_{mi} \Big([B_0]_{nj} + [B_1(\mathbf{q})]_{nj} \Big) + \big[C_{mn} \big([B_0]_{nk} + [B_1(\mathbf{q})]_{nk} \big) \eta_k + S_m^* \big] \frac{\partial [B_1(\boldsymbol{\eta})]_{mi}}{\partial \eta_j} \Big\}, \\
\frac{\partial [P_\eta]_i}{\partial q_j} &= V_0 \Big\{ C_{mn} \big([B_0]_{mi} + [B_1(\mathbf{q})]_{mi} \big) \frac{\partial [B_1(\mathbf{q})]_{nk}}{\partial q_j} \eta_k + \big[C_{mn} \big([B_0]_{nk} + [B_1(\mathbf{q})]_{nk} \big) \eta_k + S_m^* \big] \frac{\partial [B_1(\mathbf{q})]_{mi}}{\partial q_j} \Big\}, \\
\frac{\partial [P_\eta]_i}{\partial \eta_j} &= V_0 \Big\{ C_{mn} \big([B_0]_{mi} + [B_1(\mathbf{q})]_{mi} \big) \Big([B_0]_{nj} + [B_1(\mathbf{q})]_{nj} \Big) \Big\}.
\end{aligned} \tag{39}$$

The partial derivatives $\partial \mathbf{B}_1(\mathbf{d}) / \partial \mathbf{d}$ can be reduced further. It is straightforward to verify that

$$\frac{\partial [B_1(\mathbf{d})]_{mi}}{\partial d_j} = \begin{cases} [H_1]_{ji} = [H_1]_{ij}, & m = 1, \\ [H_2]_{ji} = [H_2]_{ij}, & m = 2, \\ [H_3]_{ji} = [H_3]_{ij}, & m = 3. \end{cases}$$

We may write this result in the following compact form

$$\frac{\partial [\mathbf{B}_1(\mathbf{d})]_m}{\partial \mathbf{d}} = \mathbf{H}_m, \quad m = 1, 2, 3.$$

Then we can realize immediately that

$$\frac{\partial [B_1(\mathbf{q})]_{nk}}{\partial q_j} \eta_k = \eta_k [H_n]_{kj} = [B_1(\boldsymbol{\eta})]_{nj}$$

Substituting these observations into Eq. (39) and rearranging some terms, we obtain

$$\begin{aligned}
\frac{\partial [P_q]_i}{\partial q_j} &= V_0 \Big\{ [B^\top(\mathbf{q})]_{im} C_{mn} [B(\mathbf{q})]_{nj} + \alpha_m [H_m]_{ij} - [B_1^\top(\boldsymbol{\eta})]_{im} C_{mn} [B_1(\boldsymbol{\eta})]_{nj} \Big\}, \\
\frac{\partial [P_q]_i}{\partial \eta_j} &= -V_0 \Big\{ [B_1^\top(\boldsymbol{\eta})]_{im} C_{mn} [B(\mathbf{q})]_{nj} + \beta_m [H_m]_{ij} \Big\}, \\
\frac{\partial [P_\eta]_i}{\partial \eta_j} &= +V_0 \Big\{ [B^\top(\mathbf{q})]_{im} C_{mn} [B_1(\boldsymbol{\eta})]_{nj} + \beta_m [H_m]_{ij} \Big\}, \\
\frac{\partial [P_\eta]_i}{\partial w_j} &= V_0 [B^\top(\mathbf{q})]_{im} C_{mn} [B(\mathbf{q})]_{nj},
\end{aligned} \tag{40}$$

where

$$\boldsymbol{\alpha}(\mathbf{q}) = \mathbf{C}[\mathbf{E}(\mathbf{q}) - \mathbf{E}^*], \quad \boldsymbol{\beta}(\mathbf{q}, \boldsymbol{\eta}) = \mathbf{C}\mathbf{B}(\mathbf{q})\,\boldsymbol{\eta} + \mathbf{S}^*. \tag{41}$$

We keep in mind that the computation of the tangent stiffness presented above refers to the element level. That is, the superscript (e) is expected to attach to the above expressions. Also, we point out once more that the tangent stiffness matrix degenerates to the stiffness matrix corresponding to the linear elasticity problem presented in [16] when the linearized strain is used. It can be most easily seen by identifying the matrices $\mathbf{H}_m$, $\mathbf{B}_1(\mathbf{q})$, $\mathbf{B}_1(\boldsymbol{\eta})$ in (40) to zero.

In comparing Eqs. (40), (41) and (29), we note that the element tangent stiffness derived for the truss structure and for the body under plane stress condition has the same algebraic structure. The differences are the kinematics assumptions under the continuum elements and of course the size of the computationally involved matrices. As a consequence, the derivation of formulas for the three-dimensional case can be performed following the above procedure. The tangent stiffness matrix and the force vectors have the same algebraic structure except that the B-matrix and H-matrix are computed in accordance with a three-dimensional continuum element.

4.2. Numerical example

To validate the proposed scheme numerically, we study in this subsection a plane stress problem designed to accept an exact solution. For a reference solution, let us examine a thin continuum body that occupies the domain $\Omega = [0, 1] \times [0, 1]$ in its undeformed state. The body is subject to an externally distributed load and the essential boundary conditions

$$u(X, Y) = v(X, Y) = 0 \quad \forall (X, Y) \in \partial\Omega.$$

so that the exact displacement solution is

$$u(X, Y) = X(1 - X)Y(1 - Y), \quad v(X, Y) = 0.$$

Such externally applied load is computed by a symbolic software based on the differential equations

$$\begin{aligned}
f_X &= -\Big\{ \frac{\partial}{\partial X} [(1 + u_X) S_{11} + u_Y S_{12}] + \frac{\partial}{\partial Y} [(1 + u_X) S_{12} + u_Y S_{22}] \Big\}, \\
f_Y &= -\Big\{ \frac{\partial}{\partial X} [v_X S_{11} + (1 + v_Y) S_{12}] + \frac{\partial}{\partial Y} [v_X S_{12} + (1 + v_Y) S_{22}] \Big\}.
\end{aligned}$$

The geometry of this problem is demonstrated in Fig. 10.

The stress components are computed in terms of the strains that are in turn related to the displacements. The data-driven strain solution is compared with the exact strain solution

$$\begin{aligned}
E_{11}^r &= \tfrac{1}{2}(2X - 1)(Y - 1)Y[2 + (2X - 1)(Y - 1)Y], \\
E_{22}^r &= \tfrac{1}{2}(X - 1)^2 X^2 (1 - 2Y)^2, \\
2E_{12}^r &= X(X - 1)(2Y - 1)[1 + (2X - 1)Y(Y - 1)],
\end{aligned}$$

which is plotted in Fig. 11.

In this test problem the Mooney-Rivlin model (16)–(18) is used. We specialize the stress-strain relation in the plane stress condition. In this two-dimensional problem the right Cauchy-Green tensor is reduced to

$$\mathbf{C} = \begin{bmatrix} C_{11} & C_{12} & 0 \\ C_{21} & C_{22} & 0 \\ 0 & 0 & C_{33}. \end{bmatrix}.$$

Using the incompressibility condition $I_3 = 1$, C_{33} can be related to the other components as

$$C_{33} = \frac{1}{C_{11} C_{22} - C_{12} C_{21}},$$

and hence

$$\begin{aligned}
I_1 &= C_{11} + C_{22} + \frac{1}{C_{11} C_{22} - C_{12} C_{21}}, \\
I_2 &= C_{11} C_{22} + \frac{C_{11} + C_{22}}{C_{11} C_{22} - C_{12} C_{21}} - \frac{1}{2} C_{12}^2 - \frac{1}{2} C_{21}^2.
\end{aligned}$$

Substituting this into (18) and performing the relevant differentiations, the stress-strain relation is obtained as follows

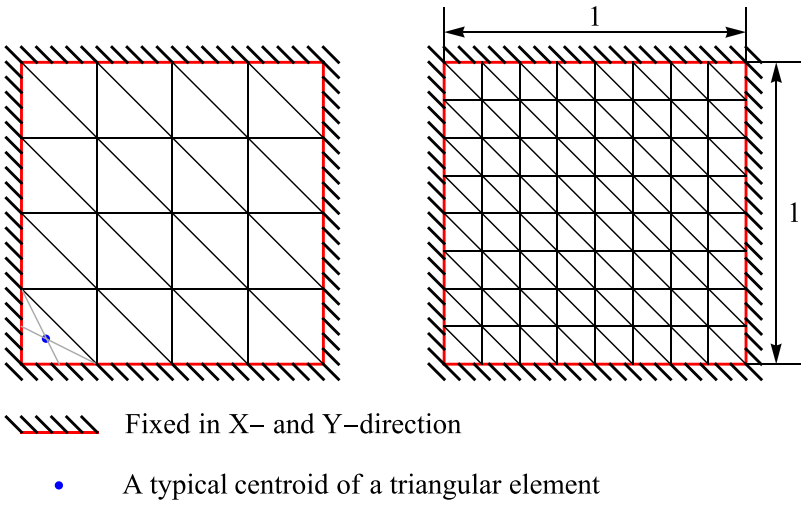

Fig. 10. Geometry of the test problem of a membrane in the plane stress condition. The finer mesh is obtained by dividing each element in the coarser mesh into four smaller elements.

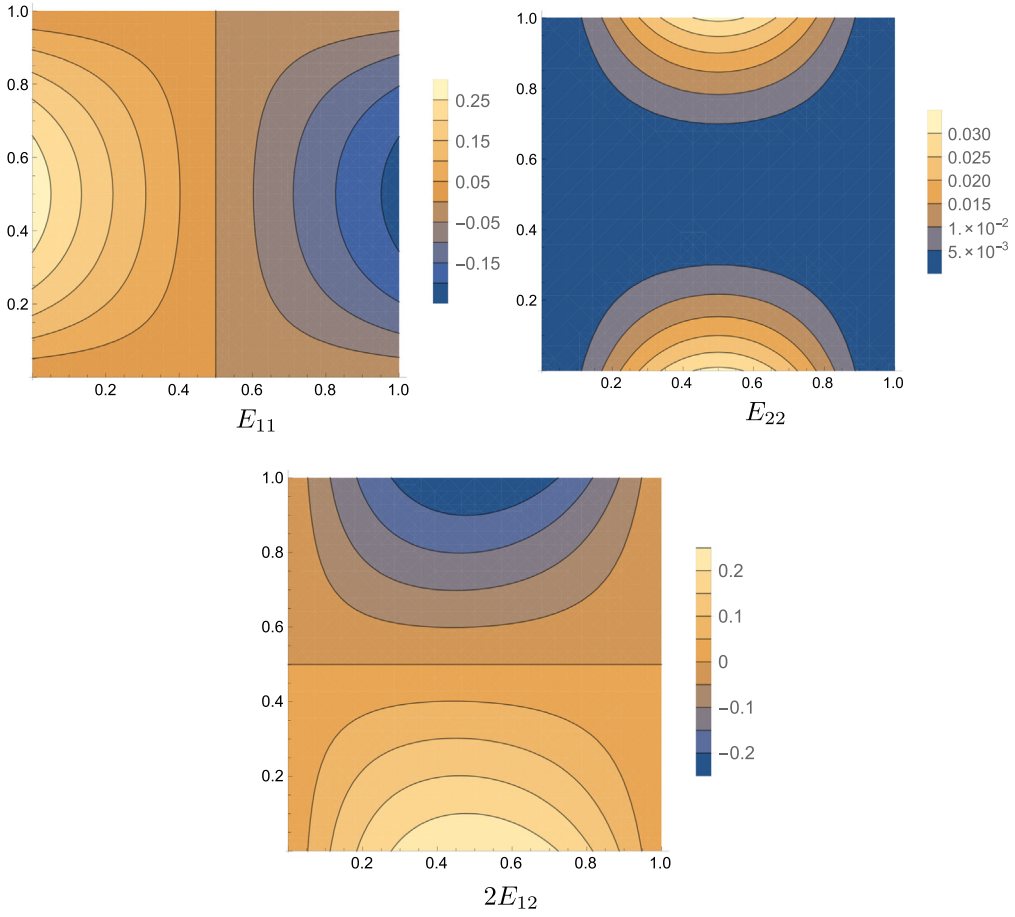

Fig. 11. Distribution of the exact strain solution of the test problem.

$$\begin{bmatrix} S_{11} \\ S_{22} \\ S_{12} \end{bmatrix} = 2C_1 \left\{ \begin{bmatrix} 1 \\ 1 \\ 0 \end{bmatrix} - C_{33}^2 \begin{bmatrix} C_{22} \\ C_{11} \\ -C_{12} \end{bmatrix} \right\} + 2C_2 \left\{ C_{33} \begin{bmatrix} 1 \\ 1 \\ 0 \end{bmatrix} + \left[1 - C_{33}^2 (C_{11} + C_{22}) \right] \begin{bmatrix} C_{22} \\ C_{11} \\ -C_{12} \end{bmatrix} \right\},$$

$$C_{ij} = 2E_{ij} + \delta_{ij}.$$

The material data sets are generated by using this stress-strain relationship.

We examine two issues in this example, namely the convergence in regard to the data size and to the mesh size. In both convergence studies, the following error metric is used

$$\frac{\|\mathbf{E} - \mathbf{E}^r\|}{\|\mathbf{E}^r\|} = \frac{\left\{ \sum_{e=1}^{N_e} \left[E_{11}\mathbf{X}_e - E_{11}^r(\mathbf{X}_e) \right]^2 + \left[E_{22}(\mathbf{X}_e) - E_{22}^r(\mathbf{X}_e) \right]^2 + \left[2E_{12}(\mathbf{X}_e) - 2E_{12}^r(\mathbf{X}_e) \right]^2 \right\}^{1/2}}{\left\{ \sum_{e=1}^{N_e} \left[E_{11}^r(\mathbf{X}_e) \right]^2 + \left[E_{22}^r(\mathbf{X}_e) \right]^2 + \left[2E_{12}^r(\mathbf{X}_e) \right]^2 \right\}^{1/2}},$$

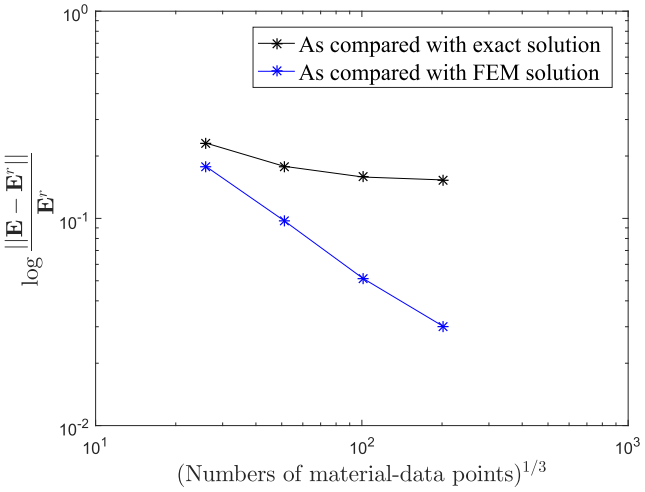

Fig. 12. Convergence of data-driven strain solution in regard to the data size.

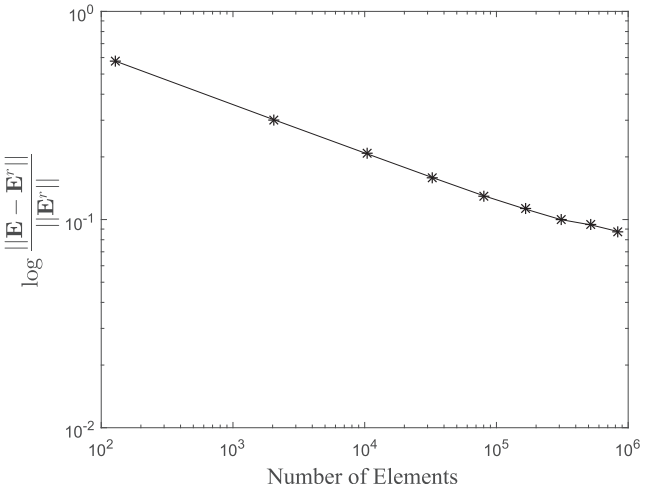

Fig. 13. Convergence of data-driven strain solution in regard to the mesh size.

where $\mathbf{X}_e = (X_e, Y_e)$ is the centroid of the e-th triangular element. In addition, we also provide the error metric that resembles the above but the reference exact strain solution evaluated at the centroids is replaced with the reference finite-element strain solution obtained by the incremental finite element procedure [25]. It is seen that as compared with the finite element solution, the relative error decreases by a half when the data set doubles it size. It is expectable as the data sets are enriched by halving the distances between the material data points and the data-driven solver has been constructed based on the finite element discretization. The results of these investigations are visualized in Figs. 12 and 13.

5. Concluding remarks

In this work we extended the data-driven computing method [16] to incorporate continuum elements within the finite deformation theory. The data-driven solver is designed to overcome the classical step of calibration of the constitutive law from the material data. Henceforth, the solver can scope not only materially nonlinear but also geometrically nonlinear problems of continuum mechanics. The patterns of the element generalized tangent stiffness and the element generalized forces are derived so that the standard finite element procedures can be easily implemented. The proposed scheme is validated through the application to various boundary-value problems. The convergence studies in regard to the mesh discretization and to the data size are conducted, which exhibits the robustness and reliability of the solver.

In spite of these good characters, the method bears some shortcomings and faces a great deal of challenges. Different employments of the collected material data may lead to different mathematical formulations although the same spirit and technique can be applied. The optimal choice of the cost function is still open to future research. The treatment of potentially inhomogeneous stress and strain states measured in an experiment requires special attention. It remains an open question how to transfer such data into the given framework, which currently relies on the (maybe hypothetical) existence of experimental data that is obtained from homogeneous tests. The use of the distance-minimizing method in combination with classical material modeling seems indispensable to push the data-driven computational mechanics towards its full potential. This is particularly true in case of inelastic material behavior.

It is clear by now that the spirit of the present work can be extended to many problems of structural mechanics such as geometrically nonlinear beam, plate and shell theories (see for example the works of Ibrahimbegovic and Frey [44] and Ibrahimbegovic [45–47]). Only the principle of virtual work taking into account the kinematics assumptions needs modification and the method of Lagrange multipliers is used to enforce the mechanical constraints.

In addition, as the material data in practice could contain noise and outliers, the data-driven computational mechanics must involve the role of statistics (see Kirchdoerfer and Ortiz [48]). Although some noise can be eliminated from the experimental point of view, the outliers may stay still in the data. In case the material data sets do not converge uniformly the data-driven solutions could be corrupted by the outliers. The distance-minimizing data-driven solver aims to find a set of material data points that most satisfy the field equations ignoring how well the material data could be clustered. Elimination of this negative effect of the data on the solutions requires statistical tools. In long-term perspective the data-driven computing techniques may find their applications when the material data can be vastly produced on a numerical basis.

Acknowledgment

The financial support of the German Research Foundation (DFG) in the framework of the *Cluster of Excellence in Simulation Technology* (EXC 310/2) at the *University of Stuttgart* is gratefully acknowledged. Furthermore, we would like to acknowledge the very constructive remarks and helpful suggestions of two anonymous reviewers of this manuscript.

References

[1] Tansley S, Tolle KM. The fourth paradigm: data-intensive scientific discovery. Microsoft Research; 2009.
[2] Bell G, Hey T, Szalay A. Computer science: beyond the data deluge. Science 2009;323:1297–8.
[3] Foreman J. Data smart: using data science to transform information into insights. John Wiley & Sons; 2013.
[4] Green AE, Zerna W. Theoretical elasticity. New York: Oxford University Press; 1954.
[5] Valanis KC, Landel RF. The strain-energy function of a hyperelastic material in terms of extension ratios. J Appl Phys 1967;38:2997–3002.
[6] Kojic M, Bathe KJ. Studies of finite element procedures-stress solution of a closed elastic strain path with stretching and shearing using the updated Lagrangian Jaumann formulation. Comp Struct 1987;26:175–9.
[7] Ogden RW. Nonlinear elastic deformations. New York: Dover Publication; 1997.
[8] Ogden RW, Saccomandi G, Sgura I. Fitting hyperelastic models to experimental data. Comput Mech 2004;34:484–502.

[9] Sussman T, Bathe KJ. A model of incompressible isotropic hyperelastic material behavior using spline interpolations of tension-compression test data. Commun Numer Meth Eng 2009;25:53–63.
[10] Kearsley EA, Zapas LJ. Some methods of measurement of an elastic strain-energy function of the Valanis-Landel type. J Rheol 1980;38:483–500.
[11] Latorre M, Rosa ED, Montáns FJ. Understanding the need of the compression branch to characterize hyperelastic materials. Int J Non-Lin Mech 2017;89:14–24.
[12] Latorre M, Montáns FJ. Extension of the Sussman-Bathe spline-based hyperelastic model to incompressible transversely isotropic materials. Comp Struct 2013;122:13–26.
[13] Latorre M, Montáns FJ. What-you-prescribed-is-what-you-get orthotropic hyperelasticity. Comput Mech 2014;53:1279–98.
[14] Latorre M, Pena E, Montáns FJ. Determination and finite element validation of the WYPIWYG strain energy of superficial Fascia from experimental data. Ann Biomed Eng 2017;45:799–810.
[15] Crespo J, Latorre M, Montáns FJ. WYPIWYG hyperelasticity for isotropic, compressible materials. Comput Mech 2017;59:73–92.
[16] Kirchdoerfer T, Ortiz M. Data-driven computational mechanics. Comp Meth Appl Mech Eng 2016;304:81–101.
[17] Ibañez R, Chavanne EA, Aguado JV, Gonzalez D, Cueto E, Chinesta F. A manifold learning approach to data-driven computational elasticity and inelasticity. Arch Comput Meth Eng 2016. http://dx.doi.org/10.1007/s11831-016-9197-9.
[18] Hashash YMA, Jung S, Ghaboussi J. Numerical implementation of a neural network based material model in finite element analysis. Int J Numer Meth Eng 2004;59:989–1005.
[19] Zopf C, Kaliske M. Numerical characterisation of uncured elastomers by a neural network based approach. Comp Struct 2017;182:504–25.
[20] Miehe C, Göktepe S, Lulei F. A micro-macro approach to rubber-line materials – part I: the non-affine micro-sphere model of rubber elasticity. J Mech Phys Solids 2004;52:2617–60.
[21] Ibrahimbegovic A, Knopf-Lenoir C, Kucerova A, Villon P. Optimal design and optimal control of structures undergoing finite rotations and elastic deformations. Int J Numer Meth Eng 2004;61:2428–60.
[22] Ibrahimbegovic A. Nonlinear solid mechanics – theoretical formulations and finite element solution methods. New York: Springer; 2009.
[23] Kalidindi SR, Niezgoda SR, Salem AA. Microstructure informatics using higher-order statistics and efficient data-mining protocols. J Miner, Metals Mater Soc 2011;63:34–41.
[24] Agarwal R, Dhar V. Big Data, Data Science, and Analytics: The Opportunity and Challenge for IS Research. Inf Syst Res 2014;25:443–8.
[25] Bathe KJ. Finite element procedures. New Jersey: Prentice Hall; 1996.
[26] Kucerova A, Brancherie D, Ibrahimbegovic A, Zeman J, Bittnar Z. Novel anisotropic continuum-discrete damage model capable of representing localized failure of massive structures–Part II: identification from tests under heterogeneous stress field. Eng Comput: Int J Comp-Aided Eng Softw 2009;26:128–44.
[27] Roweis ST, Saul LK. Nonlinear dimensionality reduction by locally linear embedding. Science 2000;290:2323–6.
[28] Johnson C. Numerical solution of partial differential equations by the finite element method. Cambridge University Press; 1988 [reprinted by Dover Publication (2008)].
[29] Brezzi F, Fortin M. Mixed and hybrid finite element methods. New York: Springer-Verlag; 1991.
[30] Douglas J, Dupont T. Superconvergence for Galerkin methods for the two point boundary problem via local projections. Numer Math 1973;21:270–8.
[31] Wahlbin LB. Superconvergence in Galerkin finite element methods. Berlin: Springer-Verlag; 1995.
[32] Ainsworth M, Oden JT. A posteriori error estimation in finite element analysis. New York: Wiley Interscience; 2000.
[33] Abramowitz M. Stegun IA. Handbook of mathematical functions with formulas, and mathematical tables – Chapter 25.4. Appl Math Ser 1983;55.
[34] Laurie DP. Computation of Gauss-type quadrature formulas. J Comput Appl Math 2001;127:201–17.
[35] Stoer J, Bulirsch R. Introduction to numerical analysis. New York: Springer; 2002.
[36] Avriel M. Nonlinear programming: analysis and methods. Dover Publications; 2003.
[37] Snyman JA. Practical mathematical optimization: an introduction to basic optimization theory and classical and new gradient-based algorithms. Springer; 2005.
[38] Mooney M. A theory of large elastic deformation. J Appl Phys 1940;11:582–92.
[39] Rivlin RS. Large elastic deformations of isotropic materials. I. Fundamental concepts. Philos Trans R Soc Lond. Ser A, Math Phys Sci 1948;240:459–90;
Rivlin RS. Large elastic deformations of isotropic materials. II. Some uniqueness theorems for pure, homogeneous deformation. Philos Trans R Soc Lond. Ser A, Math Phys Sci 1948;240:491–508;
Rivlin RS. Large elastic deformations of isotropic materials. III. Some simple problems in cylindrical polar co-ordinates. Philos Trans R Soc Lond. Ser A, Math Phys Sci 1948;240:509–25;
Rivlin RS. Large elastic deformations of isotropic materials. IV. Further developments of the general theory. Philos Trans R Soc Lond. Ser A, Math Phys Sci 1948;241:379–97.
[40] Wolfram Research, Inc., Mathematica, Version 10.3, Champaign, IL; 2015.
[41] Atkinson K. An introduction to numerical analysis. John Wiley & Sons; 1989.
[42] Wriggers P. Nonlinear finite element methods. Springer; 2008.
[43] Hughes TJR. The finite element method: linear static and dynamic finite element analysis. Dover Publications; 2000.
[44] Ibrahimbegovic A, Frey F. Finite element analysis of linear and non-linear planar deformations of elastic initially curved beams. Int J Numer Meth Eng 1993;36:3239–58.
[45] Ibrahimbegovic A. Stress resultant geometrically nonlinear shell theory with drilling rotations. Part I: a consistent formulation. Comp Meth Appl Mech Eng 1994;118:265–84.
[46] Ibrahimbegovic A. On finite element implementation of Reissner's geometrically nonlinear beam theory: three-dimensional curved beam elements. Comp Meth Appl Mech Eng 1995;122:11–26.
[47] Ibrahimbegovic A. On the choice of finite rotation parameters. Comp Meth Appl Mech Eng 1997;149:49–71.
[48] Kirchdoerfer T, Ortiz M. Data driven computing with noisy material data sets, arXiv:1702.01574.